Available online at www.sciencedirect.com
ScienceDirect
Earth-Science Reviews 78 (2006) 27–57
EARTH-SCIENCE REVIEWS
www.elsevier.com/locate/earscirev

Evolution of Tethyan phosphogenesis along the northern edges of the Arabian–African shield during the Cretaceous–Eocene as deduced from temporal variations of Ca and Nd isotopes and rates of P accumulation

D. Soudry [a,*], C.R. Glenn [b,1], Y. Nathan [a,2], I. Segal [a,2], D. VonderHaar [b,1]

[a] *Geological Survey Israel, 30 Malkhe Israel St., Jerusalem 95501, Israel*
[b] *Department of Geology and Geophysics, University of Hawaii, Honolulu, Hawaii 96822, USA*

Received 19 September 2005; accepted 27 March 2006
Available online 15 May 2006

Abstract

The evolution of Tethyan phosphogenesis during the Cretaceous–Eocene is examined to try to explain fluctuations of phosphogenesis through time, and whether or not they reflect long-term changes in ocean circulation or in continental weathering. Twenty-seven time-stratigraphic phosphate levels in various Tethyan sites, covering a time span of about 90 Myr from the Hauterivian to the Eocene, were analyzed for $^{44}Ca/^{42}Ca$ and $^{143}Nd/^{144}Nd$ in their carbonate fluorapatite (CFA) fraction. P and Ca accumulation rates and bulk sedimentation rates were quantified throughout the Cretaceous–Eocene Negev sequence to examine how changes in $^{44}Ca/^{42}Ca$ and $^{143}Nd/^{144}Nd$ are reflected in the intensity of phosphogenesis.

A clear-cut change occurs in $\varepsilon_{Nd(T)}$ and $\delta^{44}Ca$ and in the rates of P and Ca accumulation and bulk sedimentation through the time analyzed. $\varepsilon_{Nd(T)}$ is much lower in the Hauterivian–Lower Cenomanian (−12.8 to −10.9) than in the Upper Cenomanian–Eocene (−7.8 to −5.9). Much lower $\delta^{44}Ca$ values occur in the Hauterivian–Turonian (−0.22 to +0.02) than in the Coniacian–Eocene (+0.23 to +0.40). P accumulation rates in the Negev steeply increase from <200 μmol cm^{-2} k yr^{-1} in the Albian–Coniacian to ~1500 μmol cm^{-2} k yr^{-1} in the Campanian, whereas a strong decrease is concomitantly recorded in the rates of Ca accumulation and bulk sedimentation. In addition, distinct $\varepsilon_{Nd(T)}$ values are shown by the phosphorites of the Negev (−6.7 to −6.4) and Egypt (−9.1 to −7.6) during the Campanian, and by those of the Negev (−7.8 to −6.3) and North Africa (−10.1 to −8.9) during the Maastrichtian–Eocene.

The culmination of P accumulation rates in the Negev during the Campanian, occurring with a high in $\varepsilon_{Nd(T)}$ and $\delta^{44}Ca$ and a low in sedimentation rates, indicates that paleoceanographic and paleogeographical factors mostly governed phosphorite accumulation in this area. The abrupt $\varepsilon_{Nd(T)}$ rise after the Cenomanian is attributed to increased incursion of Pacific (radiogenic) water masses into the Tethys, driven by the Late Cretaceous global sea-level rise, the connection between North and South Atlantic, the global post-Santonian cooling, and the progressive widening of the Caribbean threshold, all acting in combination to significantly intensify the Tethyan circumglobal current (TCC). It also reflects a weakening of the continental Nd signal due to a reduction of exposed landmasses caused by increased flooding of continental shelves. High $\delta^{44}Ca$ values at those times also point to a decrease in weathering Ca^{+2} fluxes and expansion of carbonate sedimentation in shelves, both enriching seawater with

* Corresponding author. Fax: +972 2 5380688.
E-mail addresses: david.soudry@mail.gsi.gov.il (D. Soudry), glenn@soest.hawaii.edu (C.R. Glenn), y.nathan@mail.gsi.gov.il (Y. Nathan), irena.segal@mail.gsi.gov.il (I. Segal), denys@soest.hawaii.edu (D. VonderHaar).
[1] Fax: +1 808 956 5512.
[2] Fax: +972 2 5380688.

0012-8252/$ - see front matter
doi:10.1016/j.earscirev.2006.03.005

isotopically heavy Ca^{+2}. Deep ocean circulation intensified by the post-Santonian cooling of high latitudes increased P inventory in the Tethys basin, whereas the strengthened TCC and the folded shelf likely resulted in coastal and topographically-induced upwelling, supplying P-rich intermediate waters to southeastern Tethys shelves. Only in the Paleocene–Eocene, following major changes in global circulation produced by narrowing of Tethys and widening of the Atlantic, did phosphogenesis shifts its locus of high intensity to the western (Atlantic) Tethys and West African Atlantic coasts. This change in paleocirculation is expressed by distinctly differing $\varepsilon_{Nd(T)}$ in the Middle East and the North and West African phosphorites, suggesting different oceanic P sources and current systems for these two major groups of phosphorites. Our Nd isotope results further suggest a weaker TCC during the Mid-Cretaceous, becoming more intense in Late Cretaceous times. They also point to the North Pacific Ocean as major source of deep water formation for the intermediate–deep waters in the Tethys Basin during the Late Cretaceous.

Keywords: phosphogenesis; south Tethys margins; Cretaceous–Eocene; $\varepsilon_{Nd(T)}$; $\delta^{44/42}Ca$; P accumulation rates; paleoceanography; TCC; deep water formation

Contents

1. Introduction

Phosphorus (P), carbon (C) nitrogen (N) and potassium (K) are all nutrient elements indispensable for plant growth and animal life. In contrast to C–N and K which are virtually of unlimited availability in nature (atmosphere and seawater, respectively), P is far more restricted in nature and is available only via the exploitation of phosphate rocks (phosphorites). Apart from being the prime source of P for the phosphate fertilizer industry (main use of P), phosphorites are also of high scientific interest as they provide valuable information on the ecology and chemistry of the world's past oceans. As a limiting nutrient of living systems, P controls oceanic productivity on Earth as well as the rate of CO_2 removal from the atmosphere and the rate of marine denitrification. This links the P cycle to the carbon (C) and nitrogen (N) cycles (Mackenzie et al., 1993; Schlesinger, 1997; Arrigo, 2005), regulating in this way Earth's climate and levels of atmospheric oxygen (Van Cappellen and Ingall, 1996) and nitrogen (Falkowski, 1997) over geological time scales. The source of long term P supply to the oceanic reservoir is continental weathering of sedimentary and igneous rocks. Once extracted by planktonic organisms from the photic zone of the oceans, P is transferred to the sea bottom as part of sedimentary organic matter (OM), and a fraction of it may be fixed as authigenic carbonate fluorapatite (CFA) in bottom sediments during early diagenetic suboxic degradation of OM (Froelich et al., 1988; Glenn, 1990a). Large phosphate deposits (phosphorite "giants") were formed at several time-intervals of the Phanerozoic as the result of intensive P accumulation (Cook and McElhinny, 1979; Glenn et al., 1994). Today, marine phosphate formation is mostly restricted to a few sites in continental margins (off Peru/Chile, Baja California, Namibia) all associated with intense coastal upwelling and resulting high productivity.

Fundamental uncertainties remain about the apparent discontinuity of phosphogenesis through time (e.g., Sheldon, 1980; Baturin et al., 1995; Föllmi, 1996). Cook and McElhinny (1979), following Sheldon (1964), linked temporal variations in phosphogenesis to global changes in paleogeography and paleoceanography (see also Arthur and Jenkyns, 1981; Riggs, 1984) related to plate tectonic re-organization. For phosphogenesis to start, continents had to be in low latitudes and seaways had to be wide enough (Cook and McElhinny, 1979) to enable sufficient marine circulation for substantial oceanic upwelling. As in modern situations (e.g., Baturin, 1982; Thiede and Suess, 1983; Garrison and Kastner, 1990), coastal upwelling will supply nutrient-rich waters to continental margins, increasing primary production and P transfer to the sea bottom in these zones. Indeed, a number of major phosphate occurrences in the geological past are associated with positive $\delta^{13}C$ shifts indicating increased productivity and organic carbon burial (e.g., Kump, 1990; Compton et al., 1990; Mallinson and Compton, 1997). Many have used this model to explain phosphogenesis in the past, for example the Permian Phosphoria Formation (McKelvey et al., 1959; Hiatt and Budd, 2003), the Late Cretaceous phosphorites of the Negev (Kolodny, 1980; Reiss, 1988; Almogi-Labin et al., 1993), NW Europe (Jarvis, 1992), and Colombia (Föllmi et al., 1992), the Early Eocene Moroccan phosphorites (Slansky, 1980), the Miocene phosphorites of Florida (Compton et al., 1993) and North Carolina (Riggs et al., 1990), and the Monterey Miocene phosphorites (Garrison et al., 1990).

Yet, quite different views have evolved during the last few years concerning phosphorite formation. Central to these is the view that upwelling oceanic circulation may not be a necessary prerequisite to produce the huge P accumulation of the past, that P burial rates via authigenic CFA formation are rather constant over geological times, and also that continental weathering may directly control rates of phosphogenesis on shelves (e.g., Barron and Frakes, 1990; Glenn and Arthur, 1990; Delaney and Filippelli, 1994; Ilyin, 1994). Global warming at times of sea-level rises will lead to enhanced chemical weathering of the hinterland, causing high supply of continental P to the shelves and increased phosphate formation. Reviving earlier views (Bushinski, 1966), Ruttenberg and Berner (1993) also claimed that phosphorite episodicity is more a reflection of appropriate depositional settings (causing local secondary concentration of disseminated, previously-formed apatite; see also Filippelli, 2004) than the result of increased P removal from the ocean reservoir.

We use the Cretaceous–Eocene of the Negev (southern Israel) and of other sites in south Tethys margins as a representative geological time-window, widening the results of an earlier preliminary study (Soudry et al., 2004), to try to shed more light on this controversial question. This area along the northern edges of the Arabian–Nubian shield was the site of intense phosphogenesis during the Late Cretaceous–Eocene, containing $\sim 29 \times 10^9$ t of phosphate rocks (Jasinski, 2003), more than half of the world's phosphate resources. The Cretaceous–Eocene is also a period of major climatic, tectonic, and paleogeographic changes and therefore is highly appropriate for such a study. We measured the isotopic compositions of Ca and Nd in CFA occurrences throughout this geological interval, and examined how these compositions vary with concomitant changes in P and Ca accumulation and in rates of bulk sedimentation.

Studies in marine carbonates (Shaw and Wasserburg, 1985; Fanton et al., 2002) and phosphates (e.g., Grandjean et al., 1987; Stille et al., 1996; Shields et al., 2000) showed that the Nd isotopic compositions ($^{143}Nd/^{144}Nd$) may help to decipher changes in ocean circulation and continental weathering. The $^{143}Nd/^{144}Nd$ ratio in rocks depends upon their initial Sm/Nd ratio and their age, the radiogenic isotope ^{143}Nd produced by decay of ^{147}Sm. Old continental crustal rocks contain low Sm concentrations and therefore tend to have lower $^{143}Nd/^{144}Nd$ values than younger, mantle-derived rocks (e.g., Ehrenberg and Nadeau, 2002). Most of the Nd supplied to oceans derives from continental weathering whereas only small contributions are from mantle sources (Piepgras and Wasserburg, 1982). Due to the short residence time of Nd in seawater (200–1000 yr., Tachikawa et al., 1999), compared to the ocean mixing time (~1500 yr. — Broecker et al., 1960), changes in Nd sources in seawater, or mixing of isotopically different water masses, are reflected in the Nd isotopic-stratigraphic record. Fossil phosphates are particularly adequate for tracking such past oceanic water mass exchange, as they are contain significant amounts of Nd (tens to hundreds of ppm) predominantly derived from seawater. Moreover, extremely low Nd concentrations in marine pore fluids together with its low geochemical mobility act to minimize its isotopic exchange during diagenesis (Holmden et al., 1996; Martin and Scher, 2004), preserving the seawater Nd isotopic signal in CFA.

Research on shell and bone material from modern organisms (Skulan et al., 1997; Zhu and Macdougall, 1998) together with laboratory experiments (Nägler et al., 2000) indicate that biological fixation of Ca^{+2}

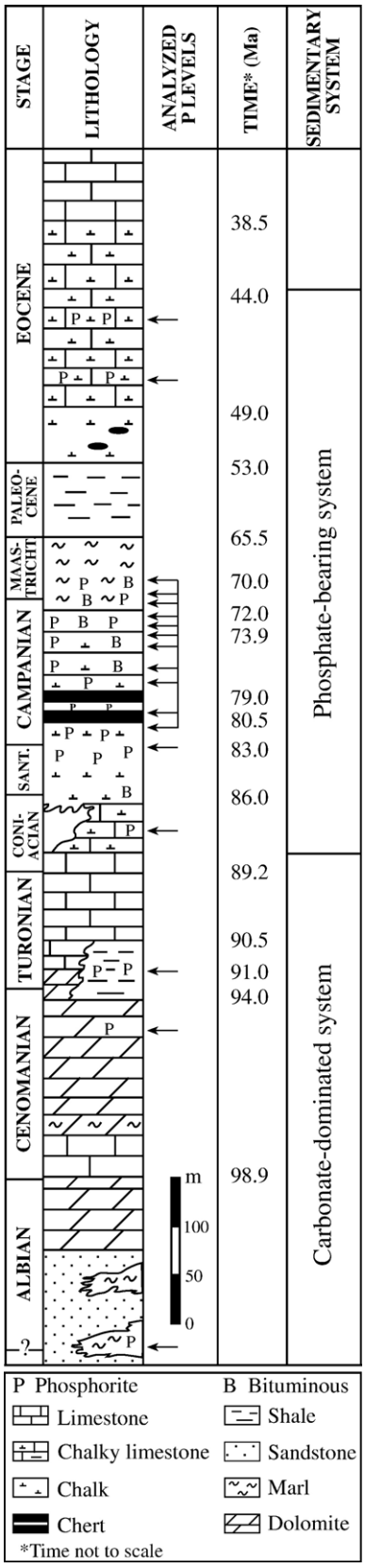

discriminates against heavy isotopes, and that this process plays an important role in regulating the isotopic composition of marine Ca^{+2}. As a result, variations in seawater isotopic Ca^{+2} are reliably recorded in biogenic carbonates (e.g., Heuser et al., 2005) and skeletal apatite as well (Skulan et al., 1997). Abundant carbonate deposition on shelves during sea-level highstands will increase the rate of biological removal of light Ca^{+2}, enriching seawater with isotopically heavy Ca^{+2}. On the other hand, increased weathering of carbonate landmasses during global sea retreats will deliver to the oceans abundant riverine Ca^{+2} enriched with the lighter Ca^{+2} isotope. High Ca concentrations (~32% in weight) in CFA should also tend to minimize isotopic exchange in diagenetic pore waters. Recent investigations (Schmitt et al., 2003b) show that pelletal phosphates also record such variations in the isotopic composition of seawater Ca^{+2}. As this composition is largely influenced by Ca^{+2} fluxes to and from the oceans (De La Rocha and DePaolo, 2000), Ca isotopic ratios in CFA can serve as a proxy for tracing changes in relative intensity of continental weathering and carbonate sedimentation through time.

2. Material

Most of the phosphate material analyzed is from the Negev and consists of phosphate samples from the Cretaceous–Eocene succession. The major part of this sequence consists of continental margin sediments deposited on a wide shelf between the open Tethys Sea to the northwest and the Arabian–Nubian Massif to the southeast. Two successive contrasting sediment-systems accumulated during this period in the Negev (Fig. 1) and in neighboring countries of the Middle East (e.g., Flexer et al., 1986; Lewy, 1990): 1) the Barremian–Coniacian, formed by partly dolomitized rudist-rich platform carbonates (Sass and Bein, 1982) together with continental sediments in the lower part (Barremian–Albian); and 2) the Upper Coniacian–Early Eocene, composed in large part of organic-rich and phosphate-bearing soft carbonates, chalks, and siliceous rocks (e.g., Bentor and Vroman, 1951; Kolodny, 1980; Benjamini, 1984; Soudry et al., 1985). This second time-interval was a period of intensive phosphogenesis in the southern edges of the Tethys ("Tethyan phosphogenesis") with massive accumulation of phosphorites in large parts of this area. Some 5.0×10^9 t of

Fig. 1. Chronostratigraphic positions of phosphate horizons (arrows) analyzed for $\delta^{44}Ca$, $^{143}Nd/^{144}Nd$, and (part of the horizons) $^{87}Sr/^{86}Sr$ along the Albian–Eocene sequence of the Negev (composite section).

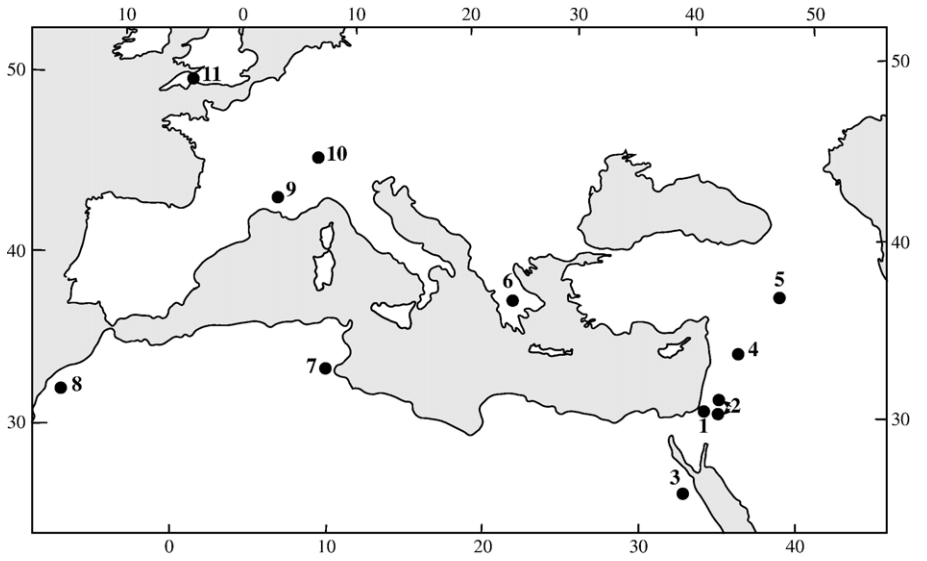

Fig. 2. Location of phosphorite samples analyzed for $\delta^{44}Ca$, $^{143}Nd/^{144}Nd$, and (part of the samples) $Sr^{87}/^{86}Sr$. 1 — Israel (Albian–Early Eocene); 2 — Jordan (Late Campanian); 3 — Egypt (Late Campanian); 4 — Syria (Late Campanian); 5 — Turkey (Turonian–Santonian); 6 — Greece (Coniacian–Santonian); 7 — Tunisia (Early Eocene); 8 — Morocco (Maastrichtian–Ypresian); 9 — SE France (Aptian–Albian); 10 — Helvetic Alps (Barremian–Albian); 11 — South England (Early Cenomanian).

phosphate rock were deposited during this period in the Middle East (Israel, Jordan, Syria and Iraq), about 1.0×10^9 t in Saudi Arabia and $\sim0.8\times10^9$ t in Egypt, whereas huge amounts ($\sim22\times10^9$ t) were deposited in the remainder of North Africa, most notably in Morocco (e.g., Jasinski, 2003).

Most of the Negev samples (Fig. 1) used for this study are unweathered drillhole material. Samples were collected from: the Coniacian–Lower Santonian (Menuha Fm.; ZS28 Zin core — Almogi-Labin et al., 1993); the Upper Campanian (Mishash Fm.; S5 Har Nishpe drillhole — Soudry and Eyal, 1994); the Maastrichtian (Ghareb Fm.; Pama B124 core; Hildebrand-Mittlefehldt, 1985); and the Early Eocene (Paran Fm.; M13 core, Mediterranean–Dead Sea hydroelectric project — Yarkoni, 1985). In stratigraphic intervals where no drillhole material was available (Albian–Turonian) we used phosphorite samples from outcrops, road cuts, and open phosphate mines.

In addition, we analyzed phosphates from the Cretaceous–Eocene in other parts of the continental Tethys margins (Fig. 2): the Maastrichtian–Ypresian phosphate-bearing suite (Ganntour deposit), Morocco (Prévôt, 1988); the Duwi Group (Upper Campanian), Egypt (Glenn and Arthur, 1990); the Amman Formation (Upper Campanian), Jordan (Abed, 1994); the Sawwaneh Formation (Upper Campanian), Syria (Al-Maleh and Mouty, 1994); the Karababa Formation (Turonian–Santonian), Turkey (Berker, 1989); the Vigla Formation (Coniacian–Santonian), Ionian zone, Greece (Pomini-Papaioannou, 2001); the "Blue Marls" (Aptian–Albian) of the Vocontian Basin, SE France (Bréhéret, 1988); and the Kieselkalk Formation (Middle Hauterivian), the Drusberg Formation (Early Barremian), and the Garschella Formation (Upper Aptian–Early Albian), all from the Helvetic Alps, Switzerland (Föllmi, 1989).

In total, 72 phosphate samples representing 27 time-stratigraphic phosphorite levels through the Hauterivian–Eocene (ca. 90 Ma) were analyzed for the Nd isotopic composition in their CFA phase. Of these, 61 samples were also analyzed for their $^{44}Ca/^{42}Ca$ compositions and 33 samples for their $^{87}Sr/^{86}Sr$ isotopic ratios. Apart from a few samples composed mainly of skeletal CFA, most of the phosphorites from the Coniacian–Eocene interval are in major part pelletal. By contrast, most of the samples from the Hauterivian–Turonian interval are nodular phosphates, commonly associated with starved sediment sequences and sedimentary discontinuities.

3. Methods

3.1. Separation of the CFA fraction

Separation of the CFA phase for isotopic analysis was done by two different procedures. In friable samples, phosphate pellets were hand-picked under microscope from the 150–290 μm-size P-rich fraction after wet-sieving and oven-drying. In some of these

samples, skeletal and pelletal CFA fractions were separated for distinct isotopic analysis. In cemented calcitic samples, the total CFA fraction was separated by selective dissolution of the calcite fraction with tri-ammonium citrate (TAC), after crushing the sample to 72 μm size. In case of samples containing dolomite, the sample was heated at 700 °C for one hour, washed with deionized water to remove the free MgO and CaO, then treated with TAC to remove any $CaCO_3$ still remaining in the sample. The separated CFA fraction was then dissolved in 1/3 M HNO_3 and chemically analyzed to ensure that carbonate was totally removed, and to determine the concentrations of Sr and bulk REEs including Nd and Sm. Measurement of major and minor elements was done by ICP-AES (JY-48, Jobin Yvon) and trace elements and REEs by ICP-MS (Elan 6000, PE-SCIEX).

Prior to isotopic analysis we checked possible weathering of the CFA samples from their structural CO_2 and their Sr/P and Ca/P ratios (Appendix A). Structural CO_2 (wt.%) was determined by the Guldbrandsen (1970) X-ray diffraction method, measuring the $\Delta 2\theta$ spacing between the (004) and (410) reflections, using a scan rate of 0.06 θ/min (absolute accuracy by this method is ±15 wt.%; precision better than ±5%). The samples were also inspected under SEM for their phosphate textures. Only samples showing flocculent phosphate textures typical of pristine phosphorites (e.g., Baturin, 1982; Soudry, 1987; Krajewski et al., 1994) were selected for isotopic analysis. We also used the $(La/Sm)_N$ ratio of the REEs in the CFA phase as proxy for possible weathering of the phosphorite. Normalization (N) was to the NASC composition (Gromet et al., 1984). Very low $(La/Sm)_N$ ratios (below 0.3) were considered (Reynard et al., 1999) as indicating intensive diagenesis involving continental fluids. Although this ratio was used mainly for skeletal apatites, we think that it could be indicative also in our analyzed (mostly peloidal) phosphates, especially when used in combination with other CFA parameters sensitive to weathering, such as the structural CO_2 and Sr/P and Ca/P ratios.

3.2. Sr and Nd isotope analysis

Of the powdered decalcified CFA sample 100 mg was processed with 5 mL of glacial acetic acid for partial dissolution of CFA. The acetic acid leachate was then centrifuged, dried, then redissolved in ~500 μL of quartz-distilled 6 M HCl and taken to dryness and weighed. The Sr, Rb, and bulk REEs were separated using calibrated 2 and 4 M HCl as eluents through a Bio-Rad AG50W-X8 (100–200 mesh) ion-exchange resin in quartz microcolumns. Sm and Nd were then separated from the REE fraction on quartz columns following the method of Mahoney et al. (1991) using α-HIBA (2-Hydroxyisobutyric acid) as eluent, and Bio-Rad AG50W-X8 (200–400 mesh) as ion exchange resin. After dissolution of the various separated dried fractions in 2 M HCl, Sr was measured using W filament, and Rb, Sm, and Nd using Ta filament. Both Sr and Nd blanks at the time of analysis were less than 20 pg g^{-1}. Sr and Nd isotopes were measured on a VG Sector multicollector mass spectrometer. The ratio $^{86}Sr/^{88}Sr = 0.1194$ was used for isotopic fractionation correction. The samples were run for at least 300 ratios or 15 blocks for each (Sr or Nd) element. Data were reported relative to $^{87}Sr/^{86}Sr = 0.710248 \pm 0.000018$ for the NBS 987 Sr standard, and relative to $^{143}Nd/^{144}Nd = 0.511847 \pm 0.000009$ for the La Jolla Nd standard. The numerical Sr ages of the samples were obtained from the secular evolution of marine $^{87}Sr/^{86}Sr$ of McArthur et al. (2001). The measured $^{143}Nd/^{144}Nd$ ratios were converted to:

$$\varepsilon_{Nd(T)} = \{[(^{143}Nd/^{144}Nd)_{sample(T)} / (^{143}Nd/^{144}Nd)_{CHUR(T)}] - 1]\} \times 10^4,$$

T = initial time of the samples; CHUR = chondritic uniform reservoir. (T) was obtained either from Sr isotopic measurements in the CFA samples where available (Appendix A); otherwise T was estimated from the stratigraphic positions of the samples in the time scales of Gradstein et al. (1995) and Berggren et al. (1995).

The initial $^{143}Nd/^{144}Nd_{(T)}$ of the samples and of $CHUR_{(T)}$ were calculated as follows:

$$(^{143}Nd/^{144}Nd)_{sample(T)} = (^{143}Nd/^{144}Nd)_{sample(today)} - [^{147}Sm/^{144}Nd)_{sample(today)} \cdot (\exp(\lambda_{Sm}T) - 1)],$$

$$(^{143}Nd/^{144}Nd)_{CHUR(T)} = (^{143}Nd/^{144}Nd)_{CHUR(today)} - [^{147}Sm/^{144}Nd)_{CHUR(today)} \cdot (\exp(\lambda_{Sm}T) - 1)],$$

where (λ_{Sm}) is the decay constant for $^{147}Sm = 6.54 \times 10^{-12}$ yr^{-1}. Common used values for CHUR (today): $^{143}Nd/^{144}Nd = 0.511836$; $^{147}Sm/^{144}Nd = 0.1967$ (Jacobsen and Wasserburg, 1980).

3.3. Ca isotope analysis

Of the powdered decalcified CFA samples 20 mg was dissolved in 2 mL of 1.3 M HCl, and an aliquot of 0.1–0.2 mL was put into a column (DOWEX 50 W × 8 resin, 100–200 mesh) previously washed and preconditioned by the same acid. Elution of Ca was

made by 6 M HCl. The solution was then dried and the precipitate dissolved in 8 mL of 0.1 M HNO_3. Ca isotopes were measured by using a multiple-collector inductively-coupled plasma-mass spectrometer (Nu Instruments, Wrexham, UK). In contrast to thermal-ionization mass spectrometery, ^{40}Ca cannot be measured using this new technique because it is overlapped by ^{40}Ar. We therefore used ^{42}Ca and ^{44}Ca isotopes which were measured simultaneously as described in Halicz et al. (1999), using the standard-sample-standard bracketing technique. NIST SRM 915a Standard was used for calculating $\delta^{44}Ca$. Final $^{44}Ca/^{42}Ca$ ratios comprise the results of 3 data runs, each counting 3 blocks of 10 ratio measurements (i.e., 90 ratio measurements). The long-term external precision of $\delta^{44/42}Ca$ (2σ) was 0.1‰.

Possible effects of occluded siliciclastics (i.e., Ca originating from the detrital fraction associated with the CFA fraction) on the Ca isotope data are considered negligible for the following reasons: we used purified CFA fractions which contain an average of some 80% CFA (the remaining 20% is mainly organic matter and quartz). The analyzed CFA samples thus contain some 32% Ca originating from CFA, all being dissolved by the HCl attack. The percentage of the clay fraction in the Negev phosphorites (the majority of the samples analyzed in this study) is very low, and the main clay mineral is smectite (Nathan et al., 1979). The average Al_2O_3 and CaO concentrations of smectite are 22% and 1.2%, respectively (Weaver and Pollard, 1973, Table XXV). The average Al_2O_3 concentration in the Negev

Table 1
Sr isotopic compositions of analyzed phosphates and strontium isotope age data. U. — upper; L. — lower; Eo — Eocene; Ma — Maastrichtian; Ca — Campanian; Co — Coniacian. Mm — macrofossil molds; N — nodular; P — pelletal; S — skeletal; In — intraclast. Numerical Sr ages obtained from McArthur et al. (2001; Version 3, updated 2000)

Sample[a] no.	Str.	CFA phase	CO_2 (wt.%)	Sr/P ($\times10^{-4}$)	Ca/P	$^{87}Sr/^{86}Sr$	±2 σ ($\times10^{-6}$)		Age (Ma)	
32a/01	L. Eo	Mm	6.1	199	3.06	0.707780	14	>44.08	46.02	<47.95
S1/02a	L. Eo	N	5.3	142	2.64	0.707739	14	>49.49	50.54	<51.28
S7/02	U. Ma	P	5.3	319	2.50	0.707806	12	>66.51	66.68	<66.91
OG-4	U. Ma	N	5.3	139	2.55	0.707798	14	>66.93	67.20	<67.46
S13/02	U. Ma	P±S	5.1	145	2.62	0.707785	12	>67.92	68.21	<68.49
S6/02	L. Ma	N	5.8	102	2.70	0.707773	13	>68.80	69.05	<69.28
OG-12	L. Ma	N	6.0	151	2.57	0.707752	12	>70.12	70.31	<74.69
D8/01	L. Ma	N	6.0	145	2.58	0.707745	12	>70.47	70.64	<70.81
AT-85	L. Ma	P	3.8	153	2.69	0.707735	12	>70.92	71.08	<71.23
D26/01	L. Ma	N	5.6	221	2.77	0.707741	13	>70.66	70.82	<70.98
S10/02	U. Ca	N	5.2	220	2.59	0.707727	12	>71.24	71.38	<71.52
D9/01	U. Ca	Mm	6.1	204	2.58	0.707713	13	>71.76	71.87	<71.98
D29/01	U. Ca	N	5.9	186	2.62	0.707701	15	>72.16	71.97	<72.37
Dis 13	U. Ca	N	5.9	219	2.68	0.707710	14	>71.86	71.97	<72.08
OG-9	U. Ca	P	3.8	104	2.46	0.707708	12	>71.93	72.03	<72.14
B2/L8	U. Ca	P	4.1	142	2.53	0.707708	14	>71.93	72.03	<72.14
D12/01	U. Ca	P	5.4	113	2.40	0.707705	14	>72.03	72.13	<72.24
B2/29	U. Ca	P	n.d.	n.d.	n.d.	0.707699	15	>72.23	72.33	<72.44
D18/01	U. Ca	In	4.5	157	2.65	0.707694	15	>72.39	72.49	<72.63
B2/L7	U. Ca	P	3.8	135	2.46	0.707694	13	>72.39	72.49	<72.60
SG/40	U. Ca	P±S	3.8	153	2.56	0.707690	12	>72.52	72.62	<72.74
B2/L4	U. Ca	P	3.1	131	2.32	0.707679	14	>72.89	73.00	<73.11
B2/L2	U. Ca	P	n.d.	116	2.40	0.707670	14	>73.18	73.30	<73.42
B2/L3	U. Ca	P	3.1	114	2.36	0.707663	13	>73.41	73.54	<73.68
B2/L1	U. Ca	P	3.2	114	2.43	0.707664	14	>73.38	73.50	<73.64
SG/32	U. Ca	P±S	3.3	94	2.44	0.707638	12	>74.26	74.46	<74.85
SG/34	U. Ca	P±S	3.2	91	2.49	0.707633	12	>74.46	74.66	<74.85
SG/38	U. Ca	P±S	3.4	89	2.43	0.707624	15	>74.85	75.04	<75.21
SG/15	U. Ca	P±S	4.1	121	2.52	0.707623	14	>74.89	75.09	<75.25
SG/27	U. Ca	P±S	3.9	96	2.46	0.707617	12	>75.18	75.35	<75.52
SG/12	U. Ca	P±S	4.5	129	2.58	0.707602	12	>75.87	76.04	<76.21
6007	L. Co	P±S	2.1	172	2.65	0.707311	13	>88.60	88.79	<88.95
6014	L. Co	P±S	5.8	187	2.79	0.707310	15	>88.60	88.82	>89.01

[a] For origin of the samples see Appendix A.

phosphorites is 0.47% (Nathan et al., 1979), and thus the clay content is ~2.1% in the purified CFA fraction. Therefore, the phosphorite samples contain some 250 ppm Ca from siliciclastic material. The HCl attack dissolves at most 50% of this siliciclastic Ca. This means that we have approximately 120 ppm of siliciclastic-Ca vs. 32% of CFA-Ca (a difference of three orders of magnitude). In terms of $^{44}Ca/^{42}Ca$ ratios, the siliciclastic effect on the $\delta^{44}Ca$ results would be in the range of ±0.0001–0.00001‰ (far below 2σ).

3.4. Quantification of P and Ca accumulation rates

P and Ca accumulation rates and the sedimentation rates along the Cretaceous–Eocene Negev succession were quantified using the time scales of Gradstein et al. (1995) for the Mesozoic and Berggren et al. (1995) for the Cenozoic, and on the basis of Negev chronostratigraphic data (Lewy, 2001; Gvirtzman, 2004). Thicknesses, and P and Ca concentrations over the Albian–Eocene sediment-successions of the Negev were collected from various literature sources and from sections analyzed in this study (Soudry et al., 2005). We used 30.97 and 40.01 as atomic weights of P and Ca, respectively, and 1.2 g/cm^3 (see also Filippelli et al., 1994) as an estimate of precompaction density (d) of the carbonate–phosphate assemblage over the sedimentary succession. P and Ca accumulation rates (Φ) are expressed in μmole cm^{-2} kyr^{-1} and μmole cm^{-2} yr^{-1}, respectively, and calculated as follows:

$$\Phi = \frac{(\text{wt.\%})10^{-2} \times d \times s}{\text{aw}} \times 10^6$$

where wt.% is the weight content of P or Ca, s the post-compaction sedimentation rate over the quantified

Table 2
Mean Nd and Ca isotopic compositions of CFA samples in stratigraphic intervals along the Cretaceous–Eocene in the Negev and in some other marginal Tethyan sites. For detailed results of the samples and their origin see Appendix A. L. — lower; M. — middle; U. — upper; Eo — Eocene; Ma — Maastrichtian; Ca — Campanian; Sa–Ca* — Santonian–Campanian transition; Co — Coniacian; Tu — Turonian; Ce — Cenomanian; Alb — Albian; Apt — Aptian; Bar — Barremian; Haut — Hauterivian

Stage	T (Ma)	n [a]	$^{143}Nd/^{144}Nd$	$\pm 2\sigma$ ($\times 10^{-6}$)	$^{147}Sm/^{144}Nd$	$^{143}Nd/^{144}Nd_{(T)}$	$\varepsilon Nd_{(T)}$	n [b]	$\delta^{44/42}Ca$
L. Eo	46.0 [c]	5	0.512290	14	0.1090	0.512256	−7.5±0.2	4	0.40±0.08
	50.5 [c]	1	0.512272	10	0.1064	0.512238	−7.8±0.2	1	0.38±0.04
U. Ma	66.7 [c]	1	0.512290	10	0.1231	0.512235	−7.8±0.2	1	0.27±0.06
	67.2 [c]	1	0.512345	10	0.1124	0.512291	−6.8±0.3	n.d.	n.d.
	68.2 [c]	1	0.512371	16	0.1213	0.512317	−6.3±0.3	1	0.24±0.06
L. Ma	69.0 [c]	1	0.512316	10	0.1077	0.512259	−7.4±0.2	1	0.23±0.01
	70.3 [c]	1	0.512333	14	0.1270	0.512275	−7.1±0.3	n.d.	n.d.
	70.7 [c]	2	0.512316	13	0.1283	0.512269	−7.5±0.2	2	0.28±0.01
	71.2 [c]	1	0.512322	10	0.1210	0.512264	−7.3±0.2	2	0.36±0.09
U. Ca	72.0 [c]	9	0.512351	16	0.1189	0.512296	−6.4±0.2	6	0.38±0.04
	72.7 [c]	10	0.512357	14	0.1221	0.512298	−6.7±0.2	4	0.35±0.09
	73.5 [c]	3	0.512379	17	0.1223	0.512320	−6.2±0.2	2	0.29±0.01
	75.0 [c]	2	0.512349	17	0.1150	0.512292	−6.7±0.3	5	0.31±0.05
	78	2	0.512316	16	0.1225	0.512304	−7.5±0.3	4	0.29±0.09
L. Ca	81	1	0.512360	10	0.1173	0.512298	−6.6±0.2	1	0.01±0.11
Sa–Ca*	83	5	0.512332	10	0.1238	0.512264	−7.3±0.2	5	0.07±0.07
U. Co	86	3	0.512356	9	0.1235	0.512286	−6.8±0.2	1	0.24±0.10
L. Co	88	7	0.512350	12	0.1110	0.512289	−6.8±0.2	7	0.26±0.05
	88.9 [c]	1	0.512314	10	0.1152	0.512247	−7.6±0.2	2	0.33±0.06
M. Tu	91	3	0.512413	8	0.1302	0.512336	−5.9±0.2	3	−0.02±0.05
U. Ce	94	1	0.512413	8	0.1300	0.512333	−5.9±0.2	1	0.02±0.06
L. Ce	96	2	0.512133	10	0.1152	0.512078	−11.2±0.2	n.d.	n.d.
L. Alb	106	4	0.512155	10	0.1148	0.512078	−10.9±0.2	4	−0.06±0.05
	110	1	0.512065	12	0.1040	0.511992	−12.6±0.2	1	−0.03±0.02
U. Apt	114	2	0.512212	8	0.1095	0.512033	−10.9±0.2	1	−0.11±0.03
L. Bar	125	1	0.512083	10	0.1323	0.511975	−12.8±0.2	1	−0.22±0.04
M. Haut	130	1	0.512134	14	0.1279	0.512029	−11.9±0.3	1	−0.19±0.05

[a] Number of samples measured for $^{143}Nd/^{144}Nd$.
[b] Number of samples measured for $\delta^{44/42}Ca$.
[c] Numerical Sr ages; other ages are approximated stratigraphic ages estimated from the stratigraphic position of the samples in time scales of Gradstein et al. (1995) and Berggren et al. (1995).

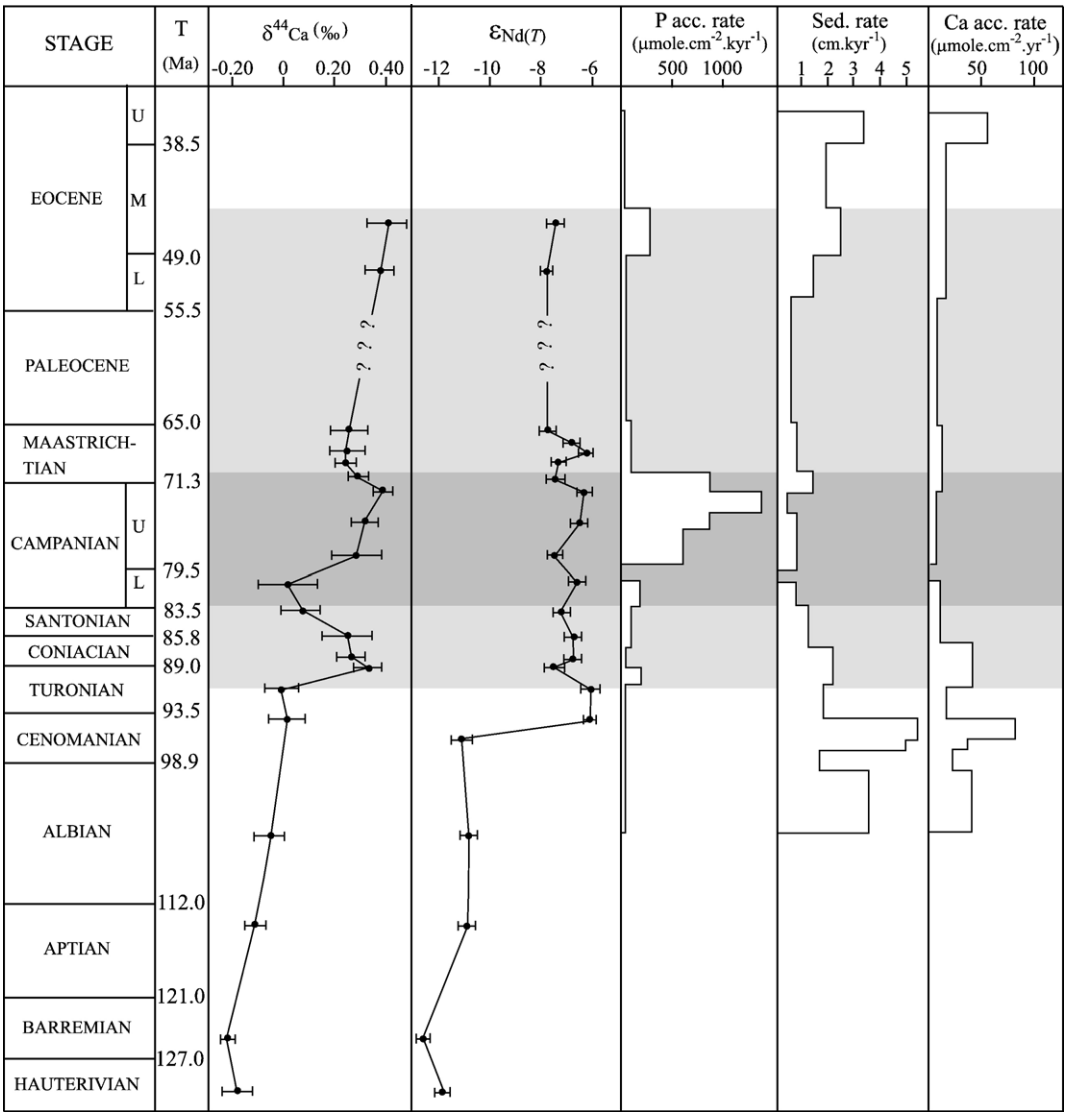

Fig. 3. Temporal evolution of δ^{44}Ca, $\varepsilon_{Nd(T)}$, P accumulation rates, sedimentation rates, and Ca accumulation rates over the examined Hauterivian–Eocene time. P and Ca accumulation rates and the bulk sedimentation rates were quantified in the Albian–Eocene Negev succession (Table 2). Maximum phosphogenesis in the Negev during the Campanian and lowermost Maastrichtian (dark grey strip) is coincident with high δ^{44}Ca and $\varepsilon_{Nd(T)}$, maximal P accumulation rates, and minimal Ca accumulation and bulk sedimentation rates. Light grey strip corresponds to the time-span during which phosphogenesis is expressed throughout the southern Tethys margins. The values plotted on the δ^{44}Ca and $\varepsilon_{Nd(T)}$ curves (part of the stratigraphic intervals in Table 1 adjacent in time were joined) are mean values of phosphate intervals along the Lower Cretaceous–Eocene and include the preliminary results in Soudry et al. (2004). Lack of Ca and Nd isotope results for the Paleocene is due to lack of suitable CFA samples in this interval. The small rise in P accumulation rates during Early Eocene reflects an additional phosphogenic episode weakly recorded in the Middle East and massively expressed in North Africa at that time.

stratigraphic interval (cm/kyr), and aw the atomic weight.

4. Results

Table 1 shows the Sr isotopic compositions of the analyzed CFA samples and the strontium isotope age data of the same samples. The results of $^{143}Nd/^{144}Nd$ and δ^{44}Ca (‰) measurements are presented in Table 2 (mean values of composite stratigraphic phosphate intervals) and detailed in Appendix A (values in individual CFA samples). The data in Appendix A also include the origin of the samples, the nature of the analyzed CFA fraction, the structural CO_2 content, and the Sr/P, Ca/P and $(La/Sm)_N$ ratios in the CFA phase.

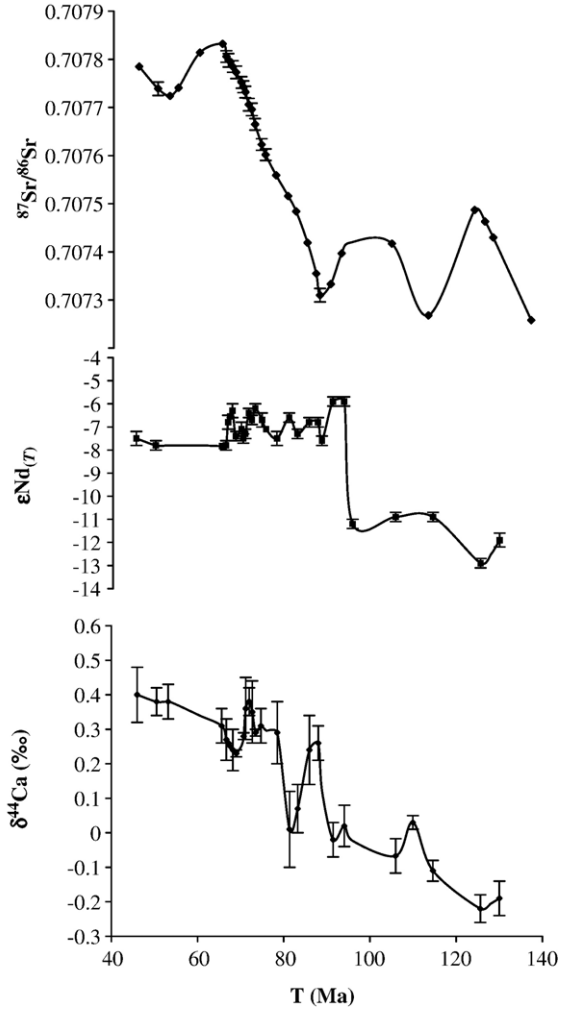

Fig. 4. Scatter diagrams of $\varepsilon_{Nd(T)}$ and $\delta^{44}Ca$ versus time (T) compared to $^{87}Sr/^{86}Sr$ over the examined Hauterivian–Eocene interval. Values with error bars correspond to measured values in the CFA samples. Points on the $^{87}Sr/^{86}Sr$ curve without error bars are non-measured values in this study and were extrapolated from the secular evolution Sr isotope curve of McArthur et al. (2001). Apart from an overall rise of both $\delta^{44}Ca$ and $^{87}Sr/^{86}Sr$ from 80 to 60 Ma, little coupling is generally observed between the geochemical evolution of $^{87}Sr/^{86}Sr$ and that of $\varepsilon_{Nd(T)}$ and $\delta^{44}Ca$ along the time examined (see also Schmitt et al., 2003b).

There is a clear-cut separation between the $\varepsilon Nd_{(T)}$ and the $\delta^{44}Ca$ (‰) compositions through the analyzed time interval (Fig. 3; Table 2). $\varepsilon Nd_{(T)}$ is much lower in the Hauterivian–Lower Cenomanian ($\varepsilon Nd_{(T)} = -12.8$ to -10.9; $n=11$) than in the Upper Cenomanian–Lower Eocene ($\varepsilon Nd_{(T)} = -7.8$ to -5.9; $n=61$). Much lower $\delta^{44}Ca$ values are also recorded in the Hauterivian–Turonian ($\delta^{44}Ca = -0.22$ to $+0.02$; $n=12$) than in the bulk of the Coniacian–Eocene ($\delta^{44}Ca = +0.23$ to $+0.40$; $n=43$). A brief lowering of $\delta^{44}Ca$ is recorded at the Santonian–Campanian transition.

P accumulation rates in the Negev (Fig. 3, Table 5) steeply increase from less than 200 μmol cm^{-2} kyr^{-1} in the Albian–Coniacian to up to ~1500 μmol cm^{-2} kyr^{-1} in the Upper Campanian–Lower Maastrichtian, decreasing to less than 100 μmol cm^{-2} kyr^{-1} in the Upper Maastrichtian, Paleocene, and the Upper Eocene. A minor P accumulation rise to ~300 μmol cm^{-2} kyr^{-1} is briefly recorded during the uppermost Lower Eocene. By contrast, both the bulk sedimentation rates and the Ca accumulation rates strongly decrease (almost by an order of magnitude) from the Albian–Santonian to the Upper Campanian, rising again in the Maastrichtian–Eocene (Fig. 3, Table 5).

Fig. 4 shows the evolution of $^{87}Sr/^{86}Sr$ through time compared with the temporal evolution of $\varepsilon_{Nd(T)}$ and

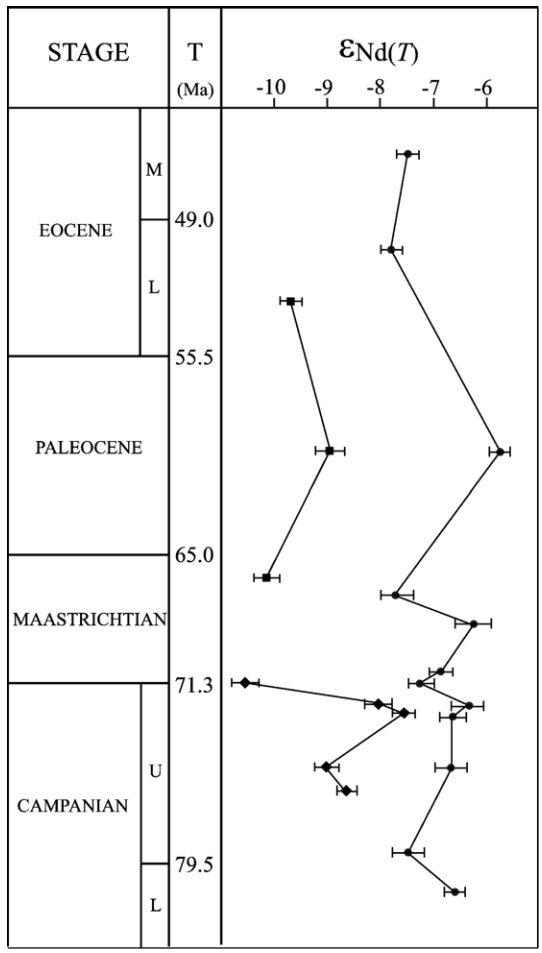

Fig. 5. $\varepsilon_{Nd(T)}$ in Negev phosphorites (circles) compared to $\varepsilon_{Nd(T)}$ values in Egypt phosphorites (diamonds) during the Campanian, and to $\varepsilon_{Nd(T)}$ values in North Africa phosphorites (squares) during the Maastrichtian–Eocene. Mantle-like $\varepsilon_{Nd(T)}$ values are recorded in Negev phosphates while more continental $\varepsilon_{Nd(T)}$ values characterize the Egypt and North Africa phosphorites in the two time-intervals (the plotted $\varepsilon_{Nd(T)}$ are mean values of several samples, see Table 3).

Table 3
Comparison of $\varepsilon_{Nd\ (T)}$ values in CFA for various Campanian–Eocene stratigraphic intervals in different south Tethys sites. Eo — Eocene; Ma — Maastrichtian; Ca — Campanian; U. — upper; L. — lower. I — Israel (Negev); II — Egypt (Red Sea coast and Western Desert); III — Morocco (Ganntour deposit). In brackets — number of samples analyzed

Stage	*T* (Ma)	I	II	III
L. Eo	46.0[a]	−7.6±0.2[b] (5)		
	50.5	−7.8±0.2 (1)		
	53			−9.7±0.2[b] (2)
	60			−8.9±0.3 (1)
U. Ma	66			−10.1±0.2[b] (3)
	66.7[a]	−7.8±0.2 (1)		
	67.2[a]	−6.8±0.3 (1)		
	68.2[a]	−6.3±0.3 (1)		
L. Ma	70.8[a]	−6.9±0.2 (1)		
	71.1[a]	−7.3±0.2 (1)	−10.6±0.2 (1)	
U. Ca	72.0[a]	−6.4±0.2[b] (7)	−8.1±0.2 (1)	
	72.5[a]	−6.7±0.2[b] (2)	−7.6±0.2 (1)	
	75.0	−6.7±0.3[b] (2)	−9.1±0.2[b] (3)	
	76.0[a]		−8.7±0.2 (1)	
	78	−7.5±0.2[b] (2)		
	81	−6.6±0.2		

[a] Sr ages; other ages are estimated stratigraphic ages.
[b] Mean values.

δ^{44}Ca. At time-points where measured $^{87}Sr/^{86}Sr$ ratios in the CFA samples are lacking, the $^{87}Sr/^{86}Sr$ values for the corresponding times (*T*) were extracted from the secular evolution Sr isotope curve of McArthur et al. (2001).

In Fig. 5 and Table 3 the $\varepsilon_{Nd(T)}$ values in the Negev phosphorites are presented compared to the values in Egyptian phosphorites during the Upper Campanian–Lower Maastrichtian, and compared to the values in North African phosphorites during the Upper Maastrichtian and the Lower Eocene. Fig. 6 shows the δ^{44}Ca evolution in the CFA samples compared with the eustatic sea level and coastal onlap (Haq et al., 1987) and with the size ($\times 10^6$ km^2) of the flooded continental areas (Ronov, 1994) during the Early Cretaceous–Eocene.

Several points emerge from the results: 1) a similar trend exists in the distribution of δ^{44}Ca and $\varepsilon_{Nd(T)}$ throughout the time analyzed (Fig. 3); 2) δ^{44}Ca and $\varepsilon_{Nd(T)}$ steeply increase after the Cenomanian–Turonian, reaching some of the highest values in the Late Campanian; 3) the δ^{44}Ca and $\varepsilon_{Nd(T)}$ highs during the Upper Campanian in the Negev coincide with a peak in rates of P accumulation and a low in rates of Ca accumulation and bulk sedimentation (Fig. 3); 4) distinct $\varepsilon_{Nd(T)}$ values characterize the phosphorites of the Negev and Egypt during the Campanian, and the phosphorites of the Negev and North Africa during the Maastrichtian–Eocene (Fig. 5); 5) overall concordant trends exist between the evolution of δ^{44}Ca, the eustatic sea-level curve, and the sizes of flooded continental areas over the analyzed Cretaceous–Eocene; 6) the evolution of Sr isotopes and that of Ca and Nd isotopes are in general largely uncoupled through the time examined.

5. Interpretation of the results and discussion

The results of Nd and Ca isotope analyses, when combined with the rates of P and Ca accumulation in the Negev and the rates of bulk sedimentation, shed more light on the development of phosphate sedimentation in this area during the Late Cretaceous. They also help to better understand the time and space migration of Tethyan phosphogenesis along the south Tethys edges during the Cretaceous–Eocene, as well as surface water circulation and the source of Tethys intermediate–deep waters at this time of major phosphate deposition.

5.1. Temporal variations of Nd isotopes

The sharp increase of $\varepsilon_{Nd(T)}$ (Table 2, Fig. 3) in the CFA samples analyzed, from very non-radiogenic (crust-like) values in the Barremian–Early Cenomanian ($\varepsilon_{Nd(T)}$ = −12.8 to −11.2) to radiogenic (Pacific-like) seawater values in the Late Cenomanian–Early Eocene ($\varepsilon_{Nd(T)}$ = −7.8 to −5.9), suggests major changes in ocean circulation and sediment deposition in the southern Tethys between these two periods. After the transgressive maximum early in the Tithonian, the global sea level fall at the Jurassic–Cretaceous transition resulted in sea regression (Haq et al., 1987) and wide exposure of land in much of Europe, the Middle East and the Arabian Peninsula (Howarth, 1981). The main exception was the central part of the Tethys which remained marine (Tyson and Funnell, 1987) with deposition of shallow-water and pelagic carbonates with some associated phosphates (e.g., Föllmi, 1989). In NW Europe (e.g., south England, Paris Basin, north Germany, the north Netherlands) this extensive regressive event is expressed by the brackish-deltaic and fluvio-lacustrine clastics (Berriasian–Barremian) of the Purbecko–Wealdian facies (e.g., Allen and Wimbledon, 1991; Ruffell, 1995). In the northwest margins of the Arabian craton this continental episode (Neocomian–Lower Aptian) is represented by massive terrigenous deposits (Kurnub Group) in Israel (Weissbrod and Perath, 1990), Jordan (Amireh, 1997), Saudi Arabia (Moshrif, 1980), Lebanon and Syria (Dubertret, 1955). In Egypt it is represented by abundant siliciclastics (Issawi, 1973) extending to the North African shelf (Klitzsch and Squyres, 1990). This extensive Early

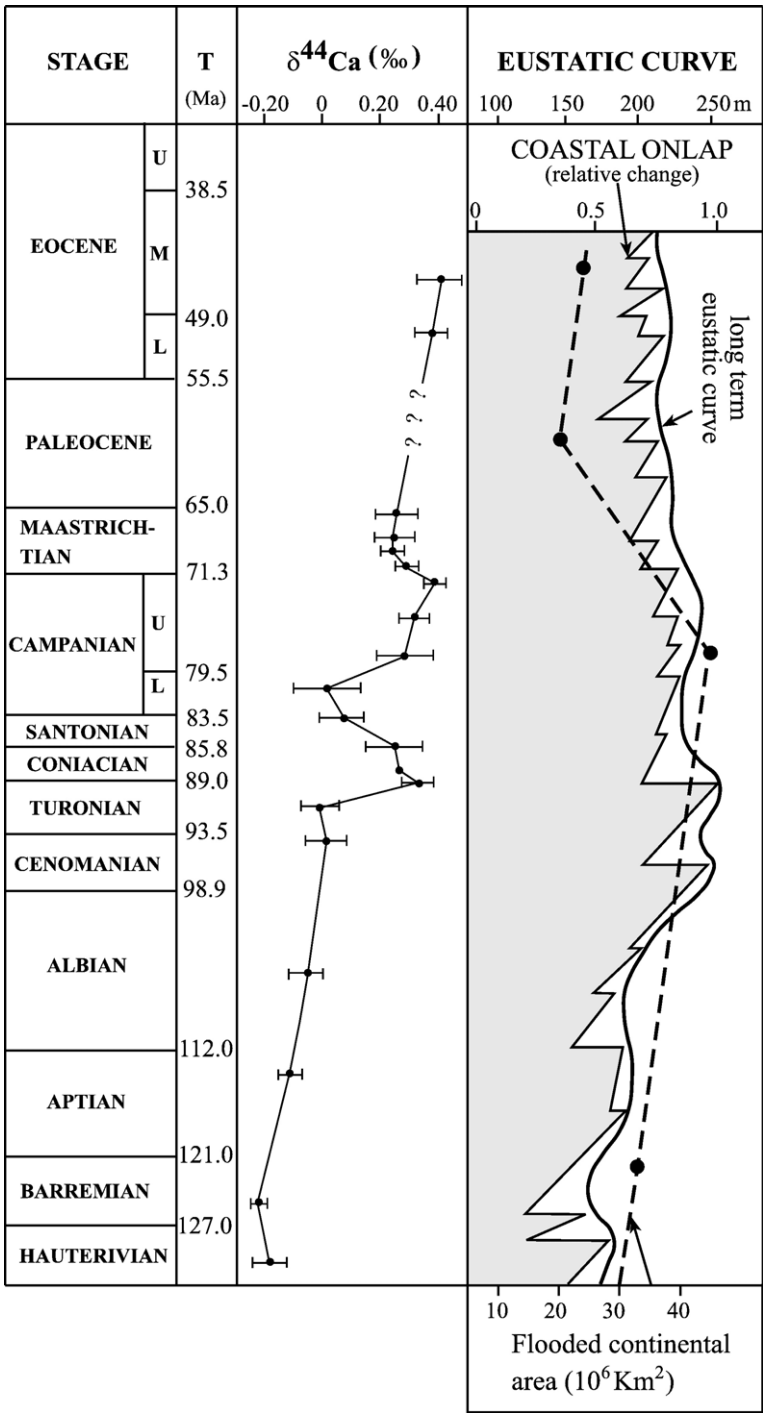

Fig. 6. Temporal evolution of $\delta^{44}Ca$ in CFA during the Early Cretaceous–Eocene. Compared with eustatic sea level and coastal onlap (Haq et al., 1987) and size (10^6 Km^2) of the flooded continental areas (Ronov, 1994) during the same time-period. More or less concordant trends are displayed by $\delta^{44}Ca$ changes and variations in continental flooding through the examined time.

Cretaceous fluvial sedimentation in the southeastern Tethys and North African shelves resulted from orogenic movements in this area at the end of the Jurassic–Middle Berriasian in connection with the breakup of Pangea (e.g., Hendriks et al., 1990). Intense erosion of the uplifted old cratonic areas resulted in thick (up to hundreds of meters) continental deposits in large parts of the south Tethys shelves (Mateer et al., 1992). The Mid-

Cretaceous was also a warm period (Wilson and Norris, 2001; Schouten et al., 2003) with a highly accelerated hydrologic cycle (Barron et al., 1989) that probably led to intense chemical weathering of exposed landmasses (e.g., Föllmi et al., 1994). Oxygen isotope analyses of planktonic foraminifera indicate sea surface temperatures as high as 30 °C in low latitudes during the Mid-Cretaceous (Huber et al., 1995; Price et al., 1998). These high temperatures are generally attributed to high levels of atmospheric greenhouse gas (Crowley, 1991; Winterer, 1991; Larson and Erba, 1999) caused by the intense mid-plate Pacific volcanism during this time (e.g., Watts et al., 1980). High chemical weathering rates and drainage from adjacent old landmasses probably resulted in high inputs of non-radiogenic Nd into the Tethys basin during the Mid-Cretaceous, explaining the low $\varepsilon_{Nd(T)}$ (as low as −12.9) in the phosphate samples of this period (Table 2, Fig. 3). Highly negative $\varepsilon_{Nd(T)}$ values, as low as −10.2 (Pucéat et al., 2005) and −8.7 (Stille et al., 1996), were also found in phosphates of the Albian of western Europe, although slightly higher (more radiogenic) values ($\varepsilon_{Nd(T)}$=−8.7 to −7.7) are also recorded in the Valanginian–Hauterivian (Pucéat et al., 2005).

In contrast to Tethys, mid-plate volcanism in the Middle Cretaceous undoubtedly produced abundant release of radiogenic (hydrothermal) Nd ($\varepsilon_{Nd(0)}$ ~ 0 to +10; Amakawa et al., 2004) to the Pacific Ocean. Between 120 and 80 Ma, Earth's oceanic crust formation increased by 50% to 75%, most of it in the Pacific Basin (Larson, 1991; Kerr, 1998). Huge oceanic basalt plateaus (Ontong Java, Manihiki) reaching ~110×10^6 km^3 in volume (Larson, 1991) were produced during the Aptian–Albian in the western Pacific. From comparison with our Nd results, the Tethys basin remained in general isotopically isolated or detached from the large amounts of mantle-derived REEs injected into Pacific water masses during Mid-Cretaceous times. This is clearly indicated by the highly negative $\varepsilon_{Nd(T)}$ values in most of our CFA samples from this period (Table 2; Fig. 3). A possible (and we contend likely) cause for this disparity in Nd isotopic signatures between ocean basins could have been a relatively weak westward-flowing Tethys circumglobal current (TCC) during the Mid-Cretaceous, causing limited exchange between Pacific and Tethys waters. Although a westward flowing TCC is generally considered a major feature of the Cretaceous Tethys Ocean (e.g., Luyendyk et al., 1972; Gordon, 1973; Lloyd, 1982), the stability of this current during the Mid-Cretaceous has been questioned. On the basis of ocean circulation simulation models, Barron and Peterson (1990) argued that eastward surface flows prevailed along the northern Tethys margin during the Mid-Cretaceous. Föllmi and Delamette (1991), by contrast, provided field evidence for a "uniform and powerful" westbound current along the northern Tethys margin. More recently, ocean circulation modeling led Poulsen et al. (1998) to suggest a more complicated circulation pattern in the Mid-Cretaceous Tethys, concluding (p. 558) that "the TTC was not the constant, prevailing feature previously envisioned" and that "it was is not truly circumglobal" as it originates in the Mediterranean Tethys (p. 555). The results of Poulsen et al. (1998) also showed that surface circulation is highly sensitive to paleogeography, and that small modifications in continent geometry caused by tectonic plate movements and sea level changes, may have significantly altered the direction and strength of Tethys circulation. Thus, a relatively weak TCC during the Mid-Cretaceous causing a reduced inflow of Pacific waters into most of Tethys could account for the non-radiogenic $\varepsilon_{Nd(T)}$ compositions in most of this interval (Fig. 3). Weakening of the TCC could have been caused by a low velocity of trade winds as a result of a weak equator- to poles temperature gradient (see Parrish and Curtis, 1982) during the Mid-Cretaceous warm period. Studies of atmospheric circulation in equatorial Pacific (Molina-Cruz, 1977) and subtropical Atlantic (Sarnthein et al., 1981) during the Late Quaternary show that the trade winds are intensified during cool climatic stages and relaxed during warm stages. Moreover, the near closure of the Caribbean threshold in the Early and Mid-Cretaceous (Scotese et al., 1988; Masse et al., 1993), together with emerging blocks (Apulia, Apennine platform, Calabria) between eastern and western Tethys (the so-called "Mediterranean Seuil" — Dercourt et al., 1993), could have created topographical obstacles to the trade winds, causing a weakening of the TCC. An unstable TTC, or perhaps not truly circumglobal (Poulsen et al., 1998), would help to better explain the fluctuating $\varepsilon_{Nd(T)}$ values (~1–1.5 ε_{Nd} units) of Pucéat et al. (2005) in northern European phosphates during this period, although in certain Mid-Cretaceous intervals (e.g., Hauterivian, Early Barremian, Late Early Aptian) the TCC was probably more active (Föllmi, 1989). Due to the short oceanic residence time of Nd, fluctuations in Tethys circulation and in the rates of water exchange, or local changes in erosional inputs, would be reflected as $\varepsilon_{Nd(T)}$ oscillations in the phosphates analyzed here. Hence, some of the highly negative $\varepsilon_{Nd(T)}$ values in the Middle Hauterivian ($\varepsilon_{Nd(T)}$=−11.9) and the Early Barremian ($\varepsilon_{Nd(T)}$=−12.8) phosphates in the Helvetic shelf could have resulted from a higher influence of the Boreal current (see Föllmi, 1989). This Boreal current system along the narrow seaway (300 km wide) between Greenland and Norway in Cretaceous times (Gradstein et

al., 1999) would have introduced non-radiogenic waters from the erosion of old landmasses (Greenland, Scandinavia) and surrounding massifs (Armorican and Brabant massifs); reduced mixing with Pacific waters at those times would have resulted in such low ε_{Nd} isotopic compositions in Tethys waters. The positive Ce anomalies (up to +0.7) in many biogenic Tethyan apatites of the Mid-Cretaceous (Lécuyer et al., 2004; Table 1) also reflect this slower ocean circulation at these times, resulting in poor mixing and ventilation of the water column.

It could be argued that the weaker ocean circulation during the Mid-Cretaceous, herein deduced from the $\varepsilon_{Nd(T)}$ values, cannot be generalized for the entire Tethys basin, as the bulk of the Mid-Cretaceous samples analyzed in this study come from the northern Tethys. Little phosphate was deposited in the southern Tethys margin during the Mid-Cretaceous (see below) and thus does not allow for thoroughly checking the validity of this argument. Still, one phosphate sample available from the Lower Albian of the southern Tethys (sample D7/01, Appendix A; Fig. 1) yielded a $\varepsilon_{Nd(T)}$ composition (−10.0) very close to the $\varepsilon_{Nd(T)}$ values (−10.2 and −10.3) obtained in the northern Tethys by Pucéat et al. (2005; Table 1), indicating that at least during the Albian the northern Tethys behaved not differently from the southern Tethys in terms of seawater Nd composition.

Many (e.g., Hays and Pitman, 1973; Matsumoto, 1980) have suggested that mid-ocean ridge volume changes continuing into the Late Cretaceous (Larson, 1991) induced the worldwide oceanic transgressions of this period. Thermally-induced uplift of the Pacific lithospheric plate caused by mid-plate volcanism also likely contributed to this transgression (Schlanger et al., 1981; Courtney and White, 1986). The rise in sea level (up to +250 m in the Late Cretaceous; Haq et al., 1987; a more attenuated 100±50 m rise was recently suggested by Miller et al., 2005), leaving only few emergent areas in the Tethys seaway (Howarth, 1981), and an increased latitudinal temperature gradient caused by the global post-Santonian cooling (Barrera and Savin, 1999), would have intensified the trade winds, accelerating the TCC and incursion of radiogenic Pacific waters onto the southern margins of the Tethys basin. Simulations with a coupled atmosphere–ocean model (Bush, 1997) and a Maastrichtian paleogeography also indicate the presence of a strong westward-flowing TCC during the latest Cretaceous, as a result of open ocean gateways between the Indian, Tethys, and Pacific Oceans and easterly wind stress in low latitudes. Likewise, $\delta^{18}O$ and $\delta^{13}C$ results in benthic foraminifera also suggest vigorous ocean circulation in this period (Barrera et al., 1997) in relation to the long-term post-Santonian cooling of high-latitude waters (Huber et al., 1995). In addition, the opening of the equatorial Atlantic gateway between the North and South Atlantic around the Cenomanian–Turonian boundary would have also enhanced the westward flow of Pacific waters through the Tethys (Poulsen et al., 2003). The sharp increase in CFA $\varepsilon_{Nd(T)}$ (Fig. 3) from the Middle ($\varepsilon_{Nd(T)}$=−12.8 to −10.9) to the Late Cretaceous ($\varepsilon_{Nd(T)}$=−7.5 to −5.9) reflects this increased Tethys and Pacific water mass mixing, causing the Nd isotopic composition of Tethys waters to evolve toward more radiogenic (mantle-like) values (see also Stille et al., 1996). One might also argue that the strong $\varepsilon_{Nd(T)}$ change from the Mid- to the Late Cretaceous results from a difference in the lithology of the CFA phase, as the Mid-Cretaceous samples are mostly nodular, whereas those of the Late Cretaceous are mostly pelletal. This, however, is quite improbable. In phosphate-forming environments today, nodular and pelletal phosphorites both form in the same setting (e.g., Glenn, 1990a) and rather similar bottom sediment conditions, very close to the sediment–water interface. Moreover, coeval nodular and pelletal phosphate occurrences present in certain Late Cretaceous intervals often show very close $\varepsilon_{Nd(T)}$ compositions (see Appendix A). Furthermore, Nd in mineral phases is quite resistant to diagenetic alteration due to the very small Nd concentrations in marine porewaters and the low geochemical mobility of this element caused by its high particle reactivity (Martin and Scher, 2004). The shift of Ce anomalies in Tethyan phosphates from positive values in the Mid-Cretaceous (Lécuyer et al., 2004) to highly negative values (as low as −0.8) in the Late Cretaceous (e.g., Shemesh, 1986; Jarvis et al., 1994; Soudry et al., 2002) also point to an increasing marine circulation resulting in well-mixed and oxygenated Tethys waters during this period.

Noteworthy are the distinct $\varepsilon_{Nd(T)}$ values in the Negev and Egyptian phosphorites in the Upper Campanian–Lower Maastrichtian (75–71 Ma) phosphogenic interval of these two areas (Table 3, Fig. 5). While in the Negev $\varepsilon_{Nd(T)}$ is −6.9 to −6.4 during this period, it is much lower (−10.6 to −7.6) in Egypt. We attribute this dissimilarity in $\varepsilon_{Nd(T)}$ to local changes in the depositional conditions of the two phosphorites. The Egyptian phosphorites typically occur with abundant glauconitic sands (Glenn and Mansour, 1979; Glenn, 1990b), whereas these are totally lacking in the Negev (Nathan et al., 1979; Soudry et al., 1985; Kolodny and Garrison, 1994) as well as in other Middle East phosphate sequences, e.g., Jordan (e.g., Abed, 1994), Syria (Al-Maleh and Mouty, 1994), or Saudi Arabia (Riddler et al., 1989). The association of glauconitic sands and phosphorites in Egypt was explained (Glenn

and Arthur, 1990) by a high fluvial discharge in this area during the Late Campanian, caused by deep lateritic weathering of the Arabian–Nubian shield at that time. This fluvial supply may have been, according to Glenn (1990b) and Glenn and Arthur (1990) the major source of P for the formation of the Egyptian phosphorites. The low (crust-like) $\varepsilon_{Nd(T)}$ in the Egyptian phosphate rocks indeed indicates a terrigenous impact (and perhaps some continental P supply) in their formation. However, the more positive (mantle-like) $\varepsilon_{Nd(T)}$ in the Negev (Table 3; Fig. 5), as well as in other Middle East (e.g., Jordan, Syria) phosphorites (Appendix A), clearly indicate that little or no terrigenous influence was felt in the course of their deposition, and that the Tethys Ocean was the most likely source of their phosphorus (see below). Due to the short residence time of Nd in seawater, these distinct $\varepsilon_{Nd(T)}$ signals were kept in the two (Egypt and Middle East) groups of phosphorites, indicating different water masses at the edges of the southeastern Tethys during the Campanian. We think that the $\varepsilon_{Nd(T)}$ values of the Egyptian phosphorites likely integrate two distinct isotopic signals, a local crustal-like isotopic Nd signal from a localized fluvial discharge, probably superimposed on a more radiogenic, Pacific-derived Nd isotopic signal that characterized the southern Tethys phosphate-depositing water mass during the Campanian.

5.2. Temporal variations of Ca isotopes

The results of Nd isotopes provide some clues as to the evolution of δ^{44}Ca over the time interval examined (Table 2, Fig. 3). Data from areas of present-day phosphate formation (off Peru–Chile, Namibia, Pacific Mexican continental shelves) indicate that CFA precipitates at the topmost zone of bottom sediments together with suboxic bacterial decomposition of organic matter (Jahnke et al., 1983; Froelich et al., 1988; Glenn, 1990a). Only there, very close to the sediment–water interface (see Jarvis et al., 1994 for a review) are the appropriate conditions (fluorine supply, phosphate and carbonate ion concentrations in pore-waters) needed for CFA precipitation coincidently met. Ca^{+2} required for CFA formation could be supplied via dissolution of carbonate shells and skeletal apatite reaching the sea floor, or directly from seawater solutions permeating the bottom sediments. As Ca is strongly fractioned during biogenic mineral formation (Skulan et al., 1997; Zhu and Macdougall, 1998), these different Ca^{+2} sources involved in CFA formation probably have distinct Ca isotopic compositions. It is not easy to assess the relative shares of these two different Ca^{+2} sources (skeletal Ca^{+2} versus seawater Ca^{+2}) in the δ^{44}Ca compositions encoded in the different CFA samples. Variable mixtures of seawater Ca^{+2} and dissolved skeletal Ca^{+2} were probably involved in the precipitation of these diverse phosphate occurrences along the sediment-succession studied. Even more complicating is that many of the samples analyzed in this study are not homogenous in composition, but rather a mixture of phosphate peloids and skeletal apatite fractions, each of which may have had their own distinct initial δ^{44}Ca compositions.

In spite of these uncertainties, the magnitude of the δ^{44}Ca change (−0.26‰ to +0.52‰; Appendix A) in the analyzed succession, as well as its trend over time (Fig. 3), lead us to think that this change probably reflects temporal variations of the isotopic seawater Ca. Support for this view is provided by the results of Schmitt et al. (2003b) who found that δ^{44}Ca in Miocene phosphate varies in the same manner as the Miocene δ^{44}Ca-carbonate (De La Rocha and DePaolo, 2000), indicating that the δ^{44}Ca-phosphate is also able to record variations of the isotopic seawater Ca. As with the $\varepsilon_{Nd(T)}$ record of the phosphates, two distinct stages are seen in the temporal evolution of δ^{44}Ca in this study (Fig. 3): 1) a Mid-Cretaceous–Turonian stage with negative δ^{44}Ca values (δ^{44}Ca as low as −0.22‰ in the Hauterivian–Albian); and 2) a Coniacian–Eocene stage with positive δ^{44}Ca values (mostly between +0.30‰ and +0.40‰). These two δ^{44}Ca stages could be explained by paleogeographic and paleoceanographic changes during this time-period. Biological fixation of Ca^{+2} into carbonates during calcification is the principal (mainly ^{40}Ca) sink in oceans (Wilkinson and Algeo, 1989). Thus, high carbonate deposition rates during times of extensive continental flooding caused by sea-level highstands will enrich seawater with isotopically heavy Ca^{+2}. Conversely, times of increased weathering of carbonate landmasses during global sea retreats will supply abundant riverine Ca^{+2} enriched with the lighter Ca^{+2} isotope to the oceans. The negative δ^{44}Ca values in CFAs during the Hauterivian–Albian are attributed to high weathering Ca^{+2} fluxes caused by the sea-level lowstands during this period (e.g., Haq et al., 1987) and wide exposure of carbonate platforms. The highly negative (crust-like) $\varepsilon_{Nd(T)}$ values recorded in CFAs during the Mid-Cretaceous (Fig. 3) also attest to this intense landmass erosion during that time. The subsequent high sea-level rise in the Upper Cretaceous, reducing the exposed landmasses and expanding the areas of carbonate sedimentation in shelves, would explain the subsequent δ^{44}Ca rise during the Coniacian–Eocene (Fig. 6). Nearly 40% of the total continental area was flooded during this period of global

sea-level rise and transgression (Howarth, 1981). The pronounced δ^{44}Ca rise in the Campanian (80–72 Ma), followed by relatively persistent positive values through the Maastrichtian and the Eocene (Fig. 3), could be explained by the increasing abundance and diversification of planktonic foraminifera and coccolithophorids that produced the extensive chalk deposits of this period (e.g., Howarth, 1981; Robaszynski et al., 1988; Hay, 1995a). This, in conjunction with a much reduced Ca^{+2} weathering flux during these times, would have enriched seawater with heavier Ca^{+2}. Elevated δ^{44}Ca during the Late Campanian–Eocene (75–45 Ma) was also observed in marine carbonates (De La Rocha and DePaolo, 2000), indicating that the Ca^{+2} sedimentation flux probably exceeded the Ca^{+2} weathering flux during this time-period. However, a positive ~ +1.0‰ offset exists between the δ^{44}Ca values of our phosphates (converted to $^{44}Ca/^{40}Ca$ ratio) compared with those of coeval marine carbonates (De La Rocha and DePaolo, 2000): the phosphates are more enriched in the heavier Ca^{+2} isotope. A similar positive offset of ~0.3–0.6‰ was also found by Schmitt et al. (2003b) between phosphates and of carbonates of Miocene to present age; this shift was explained by a mineral-dependent kinetic mass fractionation during precipitation. An alternative explanation could, however, be the variable incorporation of Ca^{+2} into CFA which may have been originally derived from two different sources: a light isotopic Ca^{+2} from dissolved skeletal carbonate grains on the sea floor, and a heavier Ca^{+2} from seawater solutions bathing the bottom sediments. The ~0.3‰ to 0.6‰ positive offset in phosphates relatively to carbonates in the Miocene probably reflects variable mixtures of these two Ca^{+2} sources in their phosphates (see also Heuser et al., 2005). In this interpretation, this offset, as well as that documented in our phosphates, would indicate that in the two cases the major part of the incorporated calcium in CFA is relatively heavy seawater Ca^{+2}, itself a function of massive biogenic carbonate deposition during these times.

It could be argued that the δ^{44}Ca increase recorded during the Coniacian–Eocene results from a change in the specific Ca fractionation factor (e.g., Deyhle et al., 2002) of the various carbonate producers throughout time. Little knowledge exists regarding this question, taking into account the variety of calcareous marine species that took part in carbonate production. Considering the results of this study we think, however, that this possibility is rather improbable. The δ^{44}Ca evolution during the Late Cretaceous–Eocene is similar in trend to that of $\varepsilon_{Nd(T)}$ (Fig. 3) which also expresses a weaker Nd weathering flux over this time interval (relative to radiogenic Pacific-type inputs). Moreover, the magnitude of $^{44}Ca/^{42}Ca$ variation (up to +0.6‰; Table 1) from the Mid-Cretaceous to the Eocene (+1.2‰ in terms of $^{44}Ca/^{40}Ca$ ratio) seems too large to be attributed solely to a change in the biological fractionation factor (see De La Rocha and DePaolo, 2000).

One might also argue that the intense Pacific volcanism during the Mid-Cretaceous (Watts et al., 1980; Kaiho and Saito, 1994), rather than paleoceanographic changes caused the lower Mid-Cretaceous δ^{44}Ca. These high spreading rates would have increased Ca- for Mg exchange via hydrothermal alteration of ocean-floor basalt (Wilkinson and Algeo, 1989; Kerr, 2002). Although a light Ca^{+2} hydrothermal contribution ($\delta^{44/40}Ca = -0.63‰$ to $-1.16‰$; Schmitt et al., 2003a) is not excluded, we think, however, that this hydrothermal source was quite secondary by comparison to weathering Ca^{+2}, taking into account the extensive continental sedimentation and the intense chemical weathering (see above) during the Mid-Cretaceous. Today, the hydrothermal Ca input to the oceans is estimated to be only 35% (Wilkinson and Algeo, 1989) or even less (22%; Berner and Berner, 1995) of the total river input. Nevertheless, some contribution of light isotopic Ca to seawater could have resulted from a shallowing of the calcium carbonate compensation depth (CCD) caused by the intense Mid-Cretaceous submarine volcanism. Deep drilling results indicate a strong CCD shallowing during the Aptian–Albian (Thierstein, 1979) produced by the abundant CO_2 release during the Ontong Java/Manihiki plateau emplacement (Winterer, 1991).

Likewise, the δ^{44}Ca variations could be viewed as the reflection of seawater temperature changes throughout the time analyzed. It has been suggested (Zhu and Macdougall, 1998) that the fractionation of Ca isotopes during calcification is temperature controlled (fractionation increasing with decreasing temperature). A $\delta^{44/40}$Ca change of 0.24±0.02 per 1 °C was deduced from cultured planktonic foraminifera (Nägler et al., 2000; Hippler et al., 2002; see also Gussone et al., 2004). A much smaller $\delta^{44/40}$Ca temperature dependence (0.05 per 1 °C) was however measured in other foraminifera cultures (Deyhle et al., 2002; Eisenhauer et al., 2002), suggesting that the magnitude of Ca isotopic fractionation is perhaps also controlled by kinetic effects caused by inter-species differences and various calcification mechanisms. This temperature effect measured in laboratory experiments is however little detected in the fossil record. In the Negev sequence, δ^{18}O in *Nodosoria* shells (benthonic foraminifera with negligible "vital effect") increases by +1‰ from the Santonian to the Campanian (Almogi-Labin et al., 1993), implying a

Table 4
δ^{44}Ca values in Santonian–Campanian skeletal phosphates of the Negev. U — upper; L — lower; Ca — Campanian; Sa–Ca — Santonian–Campanian transition

Sample no.	Strat.	δ^{44}Ca
D3/01	U. Ca	0.30±0.00
34/01s	U. Ca	0.24±0.00
D15/01	U. Ca	0.29±0.12
D30/01	L. Ca	0.01±0.11
D6/01	Sa–Ca	0.04±0.04
D27/01	Sa–Ca	0.12±0.06
32/01s	Sa–Ca	0.13±0.03

drop of about 4 °C in seawater temperature through this time-interval. δ^{18}O records of planktonic foraminifera from various oceanic sites (e.g., Barrera and Savin, 1999) also indicate a global 3–5 °C decrease in sea temperatures from the Late Campanian through the Maastrichtian. A Ca isotopic fractionation, if it was temperature controlled (Nägler et al., 2000), should have shifted δ^{44}Ca of the skeletal Negev phosphates (Table 4; Appendix A) toward lower values during the Campanian. The results of our study, however, show that δ^{44}Ca does not change and even slightly increases (up to ~ +0.3‰; Table 4; Appendix A) from the Santonian to the Campanian, suggesting little temperature dependence of the Ca fractionation factor. Actually, the evolutionary δ^{44}Ca trend (Figs. 3 and 6) over the examined time-interval (negative δ^{44}Ca values in the Hauterivian–Turonian, then positive in the Coniacian–Eocene) is rather opposite to that expected if the Ca fractionation factor was chiefly controlled by temperature. Many δ^{18}O-derived palaeo-temperature records (e.g., Arthur et al., 1979; Huber et al., 1995; Clarke and Jenkyns, 1999) indicate warming during the Aptian–Turonian and cooling during the Coniacian–Maastrichtian. Our results are also in keeping with the observations of Schmitt et al. (2003b) who found no correlation between δ^{44}Ca and δ^{18}O in Miocene–Pleistocene phosphates. Furthermore, the overall concordant trends (Fig. 6) between the measured δ^{44}Ca, the eustatic sea curve (Haq et al., 1987), and the size of the flooded continental areas (Ronov, 1994) over the Cretaceous–Eocene time examined, also tend to suggest that the changes in the isotopic seawater Ca, as recorded in our analyzed CFAs, were largely influenced by long-term paleogeographic and oceanographic changes.

5.3. Variations of P accumulation: the main pulse of massive Cretaceous phosphogenesis

P accumulation rates in the Negev steeply rise from less than 200 μmol cm^{-2} k yr^{-1} in the Albian–Coniacian to up to ~1500 μmol cm^{-2} k yr^{-1} in the Campanian–Maastrichtian (Table 5, Fig. 3). This is not specific to the Negev, or the result of paleoceanographic conditions particular to this area. Phosphate-poor sediments also characterize the Mid-Cretaceous of Jordan (Amireh, 1997; Schulze et al., 2004), Egypt (Ibrahim, 2002) and Sinai (Ayyad et al., 1996), as well as of Lebanon (Massaad, 1976), Saudi Arabia (Moshrif, 1980) and North Africa (e.g., Andreu, 1989; Mateer et al., 1992), all along the southern Tethys edges. By contrast, as in the Negev, very high P accumulation rates are recorded (calculations from literature data) in the Late Campanian of many of these areas; e.g., Jordan (Phosphorite unit — Jallad et al., 1989), ~1000–1700 μmole P cm^{-2} kyr^{-1}; Syria (economic phosphorite interval — Afteh, 1989), ~1000–1400 μmole P cm^{-2} kyr^{-1}; Egypt (Abu Tartur Phosphate Member — Issawi, 1989), ~900–1800 μmole P cm^{-2} kyr^{-1}; and Saudi Arabia (Thaniyat Phosphorite Member, Maastrichtian — Riddler et al., 1989), ~900–1200 μmole P cm^{-2} kyr^{-1}. This steep increase in P accumulation rates during the Campanian, occurring in conjunction with a high in $\varepsilon_{Nd(T)}$ and $\delta^{44/42}$Ca and a low in the rate of sedimentation (Table 5, Fig. 3), suggests some linkage between these different parameters throughout the time examined. The low P accumulation rates during the Mid-Cretaceous of the Negev (less than 50 μmole P cm^{-2} kyr^{-1}), as well as in other south Tethys areas, are explained by a diminished, or perhaps not truly circumglobal (Poulsen et al., 1998), westward-flowing Tethyan current and reduced deep ocean circulation, as also suggested by the highly negative $\varepsilon_{Nd(T)}$ compositions in the analyzed CFAs and the positive Ce anomalies in many Tethyan apatites of this period (see Nd isotope section above). This westward surface flow was probably also further weakened by the near closure of the Caribbean threshold and partial obstruction of the eastern Tethys (Masse et al., 1993) by shallow blocks (Fig. 7A), causing physical obstacles and reducing the easterly wind stress. Phosphate sediments nevertheless formed during the Mid-Cretaceous in various areas along the northern Tethys margin, e.g., the Helvetic shelf (Föllmi, 1989), the Vocontian Basin (Bréhéret, 1988; Herrle et al., 2003), and the Anglo-Paris Basin (Knight, 1999). Most of these phosphates are of nodular varieties, often of solitary nature, and are typically associated with starved sediment sequences. A preponderant TCC along the Helvetic shelf (Föllmi, 1989), sediment starvation and anoxia (Bréhéret and Delamette, 1989), or a monsoonally-forced productivity (Herrle et al., 2003) were proposed for the development of these phosphatic occurrences. In terms of relative abundances, these Mid-Cretaceous phosphates along the northern Tethys margins are, however, relatively minor,

Table 5
P and Ca accumulation rates and bulk sedimentation rates over the Cretaceous–Eocene succession in the Negev area. Eo — Eocene; Pal — Paleocene; Ma — Maastrichtian; Ca — Campanian; Co — Coniacian; Tu — Turonian; Ce — Cenomanian; Alb — Albian; U. — upper; M. — middle; L. — lower. M — marly Mbr; OS — Oil Shale Mbr; Ph — Phosphorite unit; Po — Porcelanite unit; Pcarb — Phosphatic carbonate unit; A — Avnon Mbr; T — Tamar Mbr; Za — Zafit Mbr; Yo — Yorqe'am Mbr; He — Hevyon Mbr. *T* from Lewy (1990) and Gvirtzman (2004); time scales used: Gradstein et al. (1995) — Mesozoic; Berggren et al. (1995) — Cenozoic

Stage	Stratigraphy		*T* (Ma)	*n* [a]	P acc. rate (μmole cm^{-2} kyr^{-1})	Bulk sed. rate (cm kyr^{-1})	*n* [b]	Ca acc. rate (μmole cm^{-2} yr^{-1})
	Formation	Member/unit						
U. Eo	Qez'iot		38–35	2	25±10	3.3	4	52±10
M. Eo	Matred		43.7–38	5	40±20	1.4	17	12±1.2
L. Eo	Paran		49–43.7	8	300±220	2.5±1.0		
	Mor		52.3–49	4	90±40	1.3±0.6		
Pal	Taqiya		65–53	12	70±40	0.6±0.2	11	3.3±1.3
Ma	Ghareb	M	70–65	7	110±40	0.7±0.3	10	7.7±1.4
		OS	72–70	6	630±170	1.4±0.5		
U. Ca	Mishash	Ph	74–72	31	1470±650	0.4±0.2	10	3.2±1.9
		Po	75.5–74	3	930±90	0.8±0.2		
		Pcarb	79–75.5	2	630±50	0.8±0.5		
U. Co–L. Ca	Menuha	U	83–80.5	2	170±15	0.9±0.3	10	11±1.6
		L	87–83	9	115±30	1.3±0.3		
U. Tu–Co	Zihor		89–87	4	45±10	2.1±0.3	6	23±3.6
U. Tu	Gerofit		90.5–89	15	210±130	9.2±2.9	29	100±8.6
L.–M. Tu	Ora shale		94–90.5	9	35±15	1.8±0.1	10	13.9±1.3
L. Alb–U. Ce	Hazera	A+T	95.8–94	4	50±40	5.3±1.5	19	74±2.6
		Za	97–95.8	1	20	5.0	10	33±6.2
		Yo	99–96.8	4	25±15	1.6±0.7	6	16.3±6.7
		He	103 (?)–99	2	35±15	3.5	4	38±5.2

[a] Number of stratigraphic sections quantified for P accumulation and sedimentation rates.
[b] Number of stratigraphic sections quantified for Ca accumulation rate (for sources: cf. Soudry et al., 2005).

compared to the huge Upper Cretaceous phosphorite accumulations that formed along the southeastern Tethys shelves. Compilations of phosphate data from the Deep Sea Drilling Project (DSDP) and Ocean Drilling Program (ODP) nevertheless indicate a relative increase in global P accumulation rates during the Late Albian (Föllmi, 1995).

Taken together, the discussions above lead us to the interpretation that highly elevated global sea levels, increasing open oceanic exchange between the North and South Atlantic, progressive widening of the Caribbean threshold, and intensification of the trade winds by the global post Santonian cooling, acted in combination to significantly magnify the intensity of the Late Cretaceous TCC, bringing with it increased incursions of Pacific (radiogenic) waters into the Tethys (Fig. 7B). In addition, the increased latitudinal temperature gradients as a result of the post-Santonian cooling, together with enlargement of marine gateways by the Late Cretaceous sea-level highstand (Poulsen et al., 1998), would have enhanced heat transport poleward, significantly increasing intermediate–deep ocean circulation at these times. This vigorous marine circulation would have led to redistribution of dissolved P from the deep-sea water reservoir (see Hein et al., 1993; Jewell, 1995), while the strengthened TCC and favorable wind patterns (Parrish and Curtis, 1982) caused by the tectonic plate arrangement at those times (Barron et al., 1981) would have led to intense upwelling of P-rich deep waters in the eastern (Mediterranean) Tethys (Fig. 7B). The low latitude (8–15°N) of this area during the Campanian–Maastrichtian (Smith et al., 1981) would have also greatly facilitated vertical marine circulation. At low latitudes, the nutrient-rich pycnocline waters often lie at shallow depths below the euphotic zone (Hay, 1995a) and thus are more susceptible to upwell. We expect that the nutrient concentration of these waters would progressively increase during the long transit of the TCC as it makes its way around the globe (Fig. 7B). In addition, the gentle folding of the southeastern Tethys shelf as a result of the Syrian Arc tectonism (Freund, 1965) would have created obstructions to current flow, causing cyclonic circulation in shelf water. This would have resulted in topographically-induced upwelling (e.g., Blanton et al., 1981; Snyder et al., 1990), even further enhancing nutrient supply to the photic water layer along shallow shelves. Local differences in the paleogeographic setting, e.g., shelf structure, extant of connection with the open sea, or orientation of the coastlines with respect to wind patterns, might be

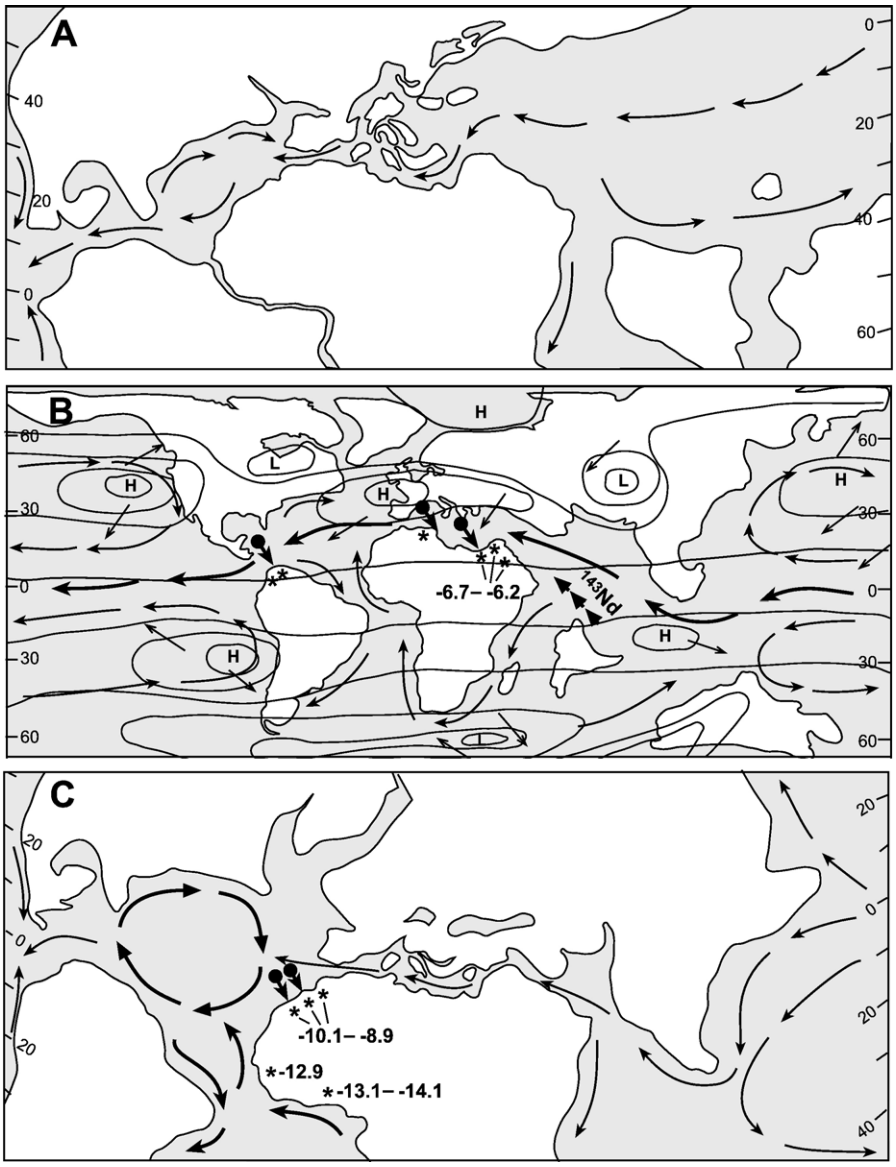

Fig. 7. Inferred development of phosphogenesis in south Tethys margins during the Mid-Cretaceous–Eocene as discussed in the text; thick arrows in bold in (B) and (C) — discussed surface paleocurrents. (A) Aptian plate tectonic reconstruction and surface paleocirculation after Masse et al. (1993), Scotese et al. (1988), and Poulsen et al. (1998, 2001). (B). Campanian–Maastrichtian plate tectonic reconstruction and surface paleocirculation from Barron (1987), Camoin et al. (1993), and Bush (1997); atmospheric cell pressures (H, L) and prevailing wind patterns (long thin arrows) from Parrish and Curtis (1982); arrow-heads points to incursion of radiogenic (^{143}Nd-rich) Pacific waters; circled-tail arrows indicate upwelling of P-rich waters; stars indicate major phosphate deposition; the mentioned values represent the range of $\varepsilon_{Nd(T)}$ in Campanian southeastern Tethys phosphates (this study). (C). Lutetian plate-tectonic reconstruction from Butterlin et al. (1993) and Scotese et al. (1988); inferred surface paleocirculation after Haq (1981). Direction of upwelling currents (circled-tail arrows) inferred from wind patterns in Parrish and Curtis (1982); stars indicate major phosphate deposition; the mentioned values represent the range of $\varepsilon_{Nd(T)}$ in Moroccan phosphates (this study) and West African phosphorites (Grandjean et al., 1987).

responsible of the changes in intensity of phosphogenesis (e.g., Slansky, 1980; Notholt et al., 1989; Lucas and Prévôt-Lucas, 1995) often observed along the southeastern edges of the Tethys during the Cretaceous.

Many studies have shown that the high latitudes were the major sites of intermediate–deep water formation during the Cretaceous, via cooling and downwelling of warm salty water flowing from the low latitudes. The North Pacific (Barron and Peterson, 1990; Li and Keller, 1999), the North Atlantic (Friedrich et al., 2004), the Southern Ocean (Brady et al., 1998; Poulsen et al., 2001; D'Hondt and Arthur, 2002), and both the North Pacific and the North Atlantic Oceans (Frank and Arthur, 1999), were proposed as deep water sources on the basis of

ocean circulation models and $\delta^{18}O$ and $\delta^{13}C$ foraminiferal records. A North Atlantic source of deep Tethys waters during the Late Cretaceous would have produced via upwelling non-radiogenic Nd isotopic compositions in the phosphates. Average ε_{Nd} of today's North Atlantic intermediate waters is −12.6, whereas it is −4 in the North Pacific waters, −8.1 in the Antarctic waters, and ranges from −7 to −10 in the Indian Ocean (Jeandel, 1993). Similar ε_{Nd} values probably also characterized these oceans during the Cretaceous (e.g., Shaw and Wasserburg, 1985; Keto and Jacobsen, 1988). As a result of considerable continental runoff, the Atlantic Ocean was also much less radiogenic than the Pacific over the last 100–150 Myr. The ε_{Nd} values of the Late Cretaceous Tethyan phosphates (−7.8 to −5.9; Table 2) preclude the possibility that the North Atlantic was a source of Tethys intermediate–deep waters. This leaves the North Pacific and the Southern Ocean as possible sites of deep water formation during the Late Cretaceous. A North Pacific Ocean source seems however more likely as the ε_{Nd} values of the phosphates are much closer to this source. Moreover, the $\delta^{13}C$ compositions of benthic foraminifera during the Late Campanian–Maastrichtian (Barrera et al., 1997; Barrera and Savin, 1999) indicate that cool waters derived more from northern than from southern high latitudes during this period.

Such cold upwelled intermediate waters flowing onto the southeastern Tethys shelves are attested by the $\delta^{18}O$ increase in Negev fish debris (Kolodny and Raab, 1988) and foraminifera (Almogi-Labin et al., 1993) of the Santonian–Campanian, even more pronounced in the phosphate-rich interval at the top of the Negev Mishash Formation (Shemesh and Kolodny, 1988). Such upwelling conditions are also evidenced by the high Cd/P ratio in the phosphorites (Nathan et al., 1997; Soudry et al., 2002), the composition of the foraminiferal (Reiss, 1988) and calcareous nannofossil (Eshet and Almogi-Labin, 1996) assemblages, as well as by the abundance of diatoms (Soudry et al., 1981; Moshkovitz et al., 1983) and infaunal deposit-feeding bivalves (Edelman-Furstenberg, 2004) in many Mishash levels. Continuous P supply to the photic zone by persistent upwelling circulation, caused by longstanding favorable marine and atmospheric circulation, probably resulted in high surface productivity and increased sea-floor phosphogenesis in the inner paleoshelf. This is attested by the very high P accumulation rates (up to ~1500 μmol cm^{-2} k yr^{-1}) in the Upper Campanian (79–72 Ma) of the Negev and other Middle East areas. The very low sedimentation rates during the Campanian of the Negev (<0.4 cm kyr^{-1}; Table 3; Fig. 3), and probably in other Middle East areas as well (e.g., Notholt et al., 1989), would have caused much of the regenerated P in bottom sediments (see Glenn, 1990a,b; Garrison et al., 1990) to be fixed as authigenic CFA. The extremely high organic C/P ratios (~1890 to 7550) in the Negev phosphorites (Nathan et al., 2006) during the Campanian attest to this intense regeneration of P from organic matter and its incorporation into authigenic CFA (see e.g., Ingall and Van Cappellen, 1989; Filippelli, 2001). The inverse correlations between the rates of P accumulation and the rates of Ca accumulation in the Negev during the Campanian (Fig. 3) are also consistent with this depositional scheme. Primary production in upwelling regions usually results in planktonic diatom blooms, due to their efficiency to compete for P and their high reproduction rates (Reiss, 1988). Such upwelling areas are contrarily less prone to calcareous nannoplankton growth (major producers of carbonates) (e.g., Pisciotto and Garrison, 1981; Isaacs et al., 1983), explaining the opposite P and Ca accumulation rates in the Negev during the Campanian (Fig. 3). Excess P availability in seawater often inhibits calcium carbonate production due to orthophosphate poisoning of calcium carbonate crystal formation (Simkiss, 1964).

By contrast, relatively little P reached the western Tethys edges (the present North Africa) during the Late Cretaceous, possibly because this area was too far from the upwelling locus situated in the eastern Tethys at that time. Due to rapid biologic uptake, upwelled waters are quickly depleted of nutrients over relatively short distances (Barber and Smith, 1981). This would have caused progressive diminishment of nutrients to upwelled waters in the TCC during its westward transport along southern Tethys. Although phosphorites also occur in the North African Maastrichtian section (Boujo, 1976; Trappe, 1991), they are however much less widespread than in the Middle East. Only in the Paleocene–Eocene (Thanetian–Ypresian), following major changes in paleocirculation did Tethyan phosphogenesis reach a high intensity in the North Africa area (Fig. 7C). The increasing plate-tectonic closure of the Tethys seaway in Paleocene–Eocene times caused by the counterclockwise rotation of Africa, together with the arrival of the Indian Plate close to Eurasia (e.g., Butterlin et al., 1993; Beck et al., 1995), probably resulted in a restriction of the Tethys circumglobal current, the main flow being shifted at the west of the Indian Plate (Haq, 1981) toward the south Indian Ocean. This, together with the increasing widening of the Atlantic Ocean, suggests that the North Africa Paleocene–Eocene phosphogenesis was, in turn, mostly fuelled by upwelling circulation from the Atlantic (Fig. 7C), and less by the TCC. This shift of oceanic P

sources from the Pacific Tethys in the Late Cretaceous to the Atlantic Ocean in the Paleocene–Eocene, is well reflected by the distinct $\varepsilon_{Nd(T)}$ compositions in the two Middle East and North Africa phosphorites. While $\varepsilon_{Nd(T)}$ is −6.3 to −7.8 (Pacific-like) in the Campanian phosphates of the Middle East, it is −8.9 to −10.1 (Atlantic-like) in the Paleocene–Eocene Moroccan phosphates (Figs. 5 and 7C; Table 3). Similar non-radiogenic $\varepsilon_{Nd(T)}$ values (−8.3 and −9.2) were also found in Late Paleocene–Early Eocene fish teeth of western (Atlantic) Tethys (Thomas et al., 2003). Less negative $\varepsilon_{Nd(T)}$ values (−5.3 to −6.9) were however reported (Grandjean et al., 1987) from a few other Moroccan phosphorites. Perhaps this scatter of $\varepsilon_{Nd(T)}$ values in the Moroccan phosphates was caused by variable admixtures of radiogenic Pacific water into the Tethys seaway during part of the Eocene, resulting in intra-basin $\varepsilon_{Nd(T)}$ differences. On the other hand, highly negative (−12.9 to −14.1) $\varepsilon_{Nd(T)}$ values (much closer to the values we measured in the Moroccan phosphates) were found (Grandjean et al., 1987 in West African (Togo, Guinea Bissau) Middle Eocene phosphorites (Fig. 7C). This change in Nd isotopic composition from the Campanian (Middle East) to the Eocene (North Africa) in the phosphorites, substantiates earlier views (Salvan, 1985) that the phosphate deposits of the Mediterranean phosphorite belt belong to two distinct phosphogenic provinces: 1) a "Tethyan" s.s. (Mesogean) province comprising the Egyptian and the Middle East Campanian phosphorites; and 2) an "Atlantic" province comprising the Moroccan phosphorites as well as the West African phosphorites (Mauritania, Senegal, Togo, Guinea Bissau) of the Eocene. Although oceanic circulation through the Atlantic was already expressed in the Cenomanian–Turonian following the connection of the North and South Atlantic (Scotese et al., 1988), only since the Maastrichtian–Paleocene was the northern Atlantic probably wide enough to enable persistent eastern boundary upwelling circulation (see Cook and McElhinny, 1979). The increasing widening of the Atlantic resulted in wide epicontinental seas along the northern African coasts with formation of extensive shelves (up to 1000 km wide along the western Sahara; Wiedmann et al., 1978). Such a paleogeographic configuration would have created in these settings the adequate oceanographic conditions for sustained upwelling and high productivity during the Paleocene–Eocene. Thus, two different oceans and traveling currents apparently fuelled phosphogenesis in the southern Tethys and in the northern Atlantic African coasts. A Tethyan flow predominant during the Late Cretaceous in the eastern (Mediterranean) Tethys (Fig. 7B), and an Atlantic flow (Stille, 1992) influencing the western (Atlantic) Tethys and the northern Atlantic African coasts during the Lower and Middle Eocene (Fig. 7C).

6. Summary and conclusions

The coupling between $\varepsilon_{Nd(T)}$, $\delta^{44}Ca$, and P accumulation rates throughout the Mid-Cretaceous–Eocene of the Negev indicate that paleoceanographic changes, rather than long-term continental weathering changes, mostly controlled the intensity of phosphogenesis in this area and probably also in others southern Tethys areas. Although the ultimate source of P is weathering of landmasses, only at times of increased ocean circulation did P become greatly available in Tethys surface waters, via its upward recycling from deeper nutrient-rich water masses. Our study also lead us to conclude that highly elevated global sea levels, increasing open oceanic exchange between the North and South Atlantic, and the progressive widening of the Caribbean threshold acted in combination to significantly magnify the intensity of the Late Cretaceous westward-flowing circumglobal Tethyan current through Tethys.

A pronounced increase in $\varepsilon_{Nd(T)}$ starting in the Late Cenomanian reflects the beginning of a marked incursion of Pacific radiogenic water masses into the Tethys seaway. It reflects a temporal change from the continental Nd isotopic signal which marked the Mid-Cretaceous in this region. A $\delta^{44}Ca$ increase during the Late Cretaceous–Eocene also reflects a decrease in weathering Ca^{+2} fluxes together with an increased biological removal of isotopically light Ca^{+2}, fostered by increased continental flooding and concomitant carbonate (chalk) carbonate sedimentation on shelves. The overall concordant trends between the measured $\delta^{44}Ca$, the eustatic sea level curve, and the sizes of the flooded continental area throughout the Early Cretaceous–Eocene, point to a linkage between the Ca isotopic composition of paleoseawater and long-term paleogeographic and oceanographic changes.

The rise in P accumulation, starting in the Coniacian and culminating in the Campanian–Maastrichtian, reflects the combined effect of the post-Santonian cooling of high latitudes, sea level highstands, and tectonic plate configuration, that stimulated the westward flowing Tethys circumglobal current and deep ocean circulation. This increased marine circulation is well imprinted in the sharp $\varepsilon_{Nd(T)}$ rise in CFAs, indicating increased water exchange between Pacific and Tethys waters. It is also reflected in the highly negative Ce anomalies in many Late Cretaceous Tethyan apatites indicating well mixed and oxygenated Tethys waters in this period. High primary productivity

and sea floor phosphogenesis prevailed mainly in the southeastern (Mediterranean) Tethys shelves as a result of persistent upwelling circulation recycling dissolved P from intermediate Tethyan waters and distributing it to the photic zone. The major source of intermediate Tethys waters during the Late Cretaceous was probably the North Pacific Ocean, as indicated by the $\varepsilon_{Nd(T)}$ compositions of the deposited phosphates. Being situated too far from the upwelling locus probably located in the eastern Tethys at that time, the western (Atlantic) Tethys (the present North Africa area) was less influenced by these nutrient-rich upwelling waters. Only in Paleocene–Eocene times, following major changes in the paleocirculation caused by the increasing plate-tectonic closure of the Tethys and widening of the Atlantic, did phosphogenesis reach high intensity in the western (Atlantic) Tethys. This shift of P oceanic sources, from the Pacific–Tethys during the Late Cretaceous to the Atlantic during the Eocene, is clearly imprinted in distinct $\varepsilon_{Nd(T)}$ compositions in the Middle East and the North and West African phosphorites.

It remains unclear however why, massive ("Giant") phosphogenesis was not triggered earlier in eastern Tethys (Middle East), despite the maximum global transgressive pulse during the Late Cenomanian (Haq et al., 1987), also recorded throughout the northern edges of the Arabo-African craton (e.g., Philip et al., 1993) and expressed in the positive $\varepsilon_{Nd(T)}$ excursion in the CFAs studied here. Paleogeographic reconstructions (Barron et al., 1981; Dercourt et al., 1993) show that the continental positions did not shift by more than a few degrees latitude from the Cenomanian to the Campanian and thus the wind patterns over the Tethys were probably quite the same (see also Parrish and Curtis, 1982). Moreover, a vigorous east-to-west equatorial flow already existed in the Tethys in Cenomanian times (Gordon, 1973; Philip et al., 1993). It is possible that the little phosphate sedimentation during the Cenomanian was due to the extreme warmth during this time interval (more than 33 °C in the upper tropical ocean — Norris et al., 2002; Schouten et al., 2003) caused by the intense greenhouse climate conditions that prevailed in this period (e.g., Larson and Erba, 1999). The latitudinal thermal gradient being at lowest during this time interval (Bice et al., 2003) perhaps caused a weakening in deep ocean circulation (Hay, 1995b) and as a result, low recycling of nutrients from the deep water reservoir. Actually, few phosphates deposits are known in the Cenomanian (e.g., Notholt et al., 1989). The only major occurrence so far reported are the nodular Cenomanian phosphorites in the East European Platform (former Soviet Union) and they were attributed to a river-P input mechanism (Ilyin, 1994). A few other minor occurrences are also known in the Lower Cenomanian of the Helvetic shelf (Föllmi, 1989) and south east England (Kennedy and Garrison, 1975).

Another possible cause for the little phosphate sedimentation during the Cenomanian could be the paleogeographic setting of the entire Levant at these times. We suggest that the general paucity of phosphorite sedimentation in this region in the Cenomanian and its later triggering in the Campanian is linked to the delicate balance between continental hypsometry and eustatic sea level, and thus relative sea level change throughout Egypt and the Levant. A huge shallow carbonate platform extended at that time between the Arabian–Nubian shield to the southeast and the open Tethys Sea to the northwest (Bein and Weiler, 1976). It is possible that the epeiric seas that covered this huge carbonate platform were not deep enough to permit the *necessary* separation of outgoing and ingoing flows, limiting upwelling circulation to more northerly open ocean conditions in the Tethys Sea, at some distance seaward of the shelf break. Only in the Late Turonian–Early Santonian, after the entire platform was changed into a subsiding ramp by the compressive deformation which affected the whole Levant (Bentor and Vroman, 1954; Bosworth et al., 1999), would the upwelled nutrient-laden waters be able to penetrate the innermost south Tethys shelves, putting an end to the carbonate platform by excess of nutrients (e.g., Kinsey and Davies, 1979; Hallock and Schlager, 1986) and initiating an unusual sedimentary regime that produces the classic upwelling triad of organic-rich, silica-rich, and phosphate-rich sediments.

Acknowledgments

This study was supported by the United States–Israel Binational Science foundation (Grant 1999232 to D. Soudry, C. Glenn and Y. Nathan), the Geological Survey of Israel (GSI Project 40030), and the University of Hawaii School of Ocean and Earth Science and Technology (Contribution No 6732). We thank Z. Lewy, A. Almogi-Labin (both of the GSI, Jerusalem), K. Föllmi (Neuchatel University, Switzerland), L. Prévôt-Lucas (Strasbourg University, France), G. Bréhéret (Tours University, France), and F. Pomini-Papaioannou (Athens University, Greece) for kindly providing phosphate samples for isotopic analysis. John McArthur (University College, London) kindly provided advise and computer look up tables for determining best fit numerical ages for our samples from comparison with the secular trends of strontium isotope seawater compositions using V3:10/99 (McArthur et al., 2001).

Sr and Nd isotopes were performed in John Mahoney's laboratories at the University of Hawaii. We also thank S. Ehrlich, D. Stieber, and O. Yoffe for carrying out the elemental geochemical analyses, N. Teplyakov for assistance in analysis of Ca isotopes, M. Dvorachek for SEM services, O. Gofin for laboratory separation of the apatite fractions, Y. Mizrahi and S. Ashkenazi for assistance in the field work, and C. Netzer-Cohen, B.-S. Cohen, and N. Shragaii (all of the GSI, Jerusalem) for their assistance in the preparation of figures. Elon Yekutieli provided useful technical support. Special thanks to Z. Lewy and A. Almogi-Labin for critically reading an earlier version of the manuscript. The comprehensive reviews of Karl Föllmi and John Compton contributed to significantly improving the manuscript.

Appendix A. Data on the analyzed phosphate samples and $^{87}Sr/^{86}Sr$, $^{143/}Nd/^{144}Nd$ and $\delta^{44/42}Ca$ compositions of the separated CFA fractions

Sample no.	Or.	Str.	T (Ma)	CFA phase	CO_2 (wt.%)	Sr/P ($\times10^{-4}$)	Ca/P	$(La/Sm)_N$	Nd ($\mu g\ g^{-1}$)	Sm ($\mu g\ g^{-1}$)	$^{143/}Nd/^{144}Nd$	$^{147}Sm/^{144}Nd$	$^{143/}Nd/^{144}Nd_{(T)}$	$\varepsilon Nd_{(T)}$	$\delta^{44/42}Ca$
OG-5	1	L. Eo.	46[a]	N	5.4	113	2.60	1.98	18.3	3.4	0.512320±16	0.1124	0.512282	−7.0±0.3	0.26±0.11
D4/01	1	L. Eo.	46[a]	Mm	3.9	167	2.59	2.94	6.6	1.1	0.512285±10	0.1008	0.512255	−7.5±0.2	0.42±0.08
D10/01	1	L. Eo.	46[a]	S	3.2	179	2.59	n.d.	1.056[b]	0.187[b]	0.512286±8	0.1071	0.512254	−7.5±0.2	n.d.
D17/01	1	L. Eo.	46[a]	N	5.7	133	2.52	2.57	10.0	1.9	0.512291± 16	0.1149	0.512256	−7.4±0.3	0.39±0.04
32a/01	1	L. Eo.	46.0[c]	Mm	6.1	199	3.06	1.99	9.9	1.8	0.512268±22	0.1100	0.512235	−7.9±0.4	0.52±0.12
S1/02a	1	L. Eo.	50.5[c]	N	5.3	142	2.64	2.47	29.0	5.1	0.512272±10	0.1064	0.512238	−7.8±0.2	0.38±0.04
S17/02	2	L. Eo.	53[a]	P	n.d.	120	2.71	1.21	19.7	4.0	0.512199±12	0.1228	0.512156	−9.4±0.2	0.27±0.03
S18/02	3	L. Eo.	53[a]	P	4.4	165	2.66	1.09	85.4	16.4	0.512164±10	0.1162	0.512124	−10.0±0.2	0.35±0.09
S19/02	2	L. Eo.	60[a]	P	2.9	121	2.39	1.92	8.6	1.6	0.512228±16	0.1125	0.512182	−8.9±0.3	0.50±0.03
S16/02	2	U. Ma.	66[a]	P	4.0	118	2.59	0.98	17.1	3.5	n.d.	n.d	n.d.	n.d.	0.36±0.12
S20/02	2	U. Ma.	66[a]	P	2.4	105	2.47	1.12	26.4	5.3	0.512198±10	0.1214	0.512146	−9.6±0.2	0.34±0.04
S29/03	2	U. Ma.	66[a]	P	2.3	121	2.52	0.88	24	4.7	0.512173±10	0.1185	0.512122	−10.1±0.2	n.d.
S30/03	2	U. Ma.	66[a]	P	2.6	132	2.57	0.83	19	3.8	0.512145±10	0.1210	0.512093	−10.6±0.2	0.23±0.01
S7/02	4	U. Ma.	66.7[c]	P	5.3	319	2.50	1.18	280	57	0.512290±10	0.1231	0.512236	−7.8±0.2	0.27±0.06
OG-4	1	U. Ma.	67.2[c]	N	5.3	139	2.55	1.48	8.4	1.7	0.512345±10	0.1124	0.512291	−6.8±0.3	n.d.
S13/02	1	U. Ma.	68.2[c]	P±S	5.1	145	2.62	1.62	37.4	7.5	0.512371± 16	0.1213	0.512317	−6.3±0.3	0.24±0.06
S6/02	1	L. Ma.	69.0[c]	N	5.8	102	2.70	2.08	59	10.5	0.512316±10	0.1077	0.512259	−7.4±0.2	0.23±0.06
OG-12	1	L. Ma.	70.3[c]	N	6.0	151	2.57	1.45	10.0	2.1	0.512333±14	0.1270	0.512275	−7.1±0.3	n.d.
D8/01	1	L. Ma.	70.6[c]	N	6.0	145	2.58	n.d.	0.520[b]	0.101[b]	0.512290±10	0.1175	0.512236	−7.8±0.2	0.28±0.01
D26/01	1	L. Ma.	70.8[c]	N	5.6	221	2.77	1.25	11	2.4	0.512342±16	0.1391	0.512282	−6.9±0.2	0.28±0.01
S5 64–65a	1	L. Ma.	71[a]	P	6.1	152	2.68	1.28	21.0	4.2	0.512322±10	0.1210	0.512264	−7.3±0.2	0.36±0.17
AT-85	5	U. Ca.	71.1[c]	P	3.8	153	2.69	0.97	205	42	0.512152±10	0.1239	0.512093	−10.6±0.2	n.d.
S10/02	1	U. Ca.	71.4[c]	N	5.2	220	2.59	1.95	7.4	1.3	n.d.	n.d.	n.d.	n.d.	0.35±0.02
D9/01	1	U. Ca.	71.9[c]	Mm	6.1	204	2.58	1.72	0.084[b]	0.016[b]	0.512205±20	0.1152	0.512151	−9.5±0.4	0.49±0.00
D29/01	1	L. Ma.	72.0[c]	N	5.9	186	2.62	1.90	8.4	1.6	0.512362±10	0.1152	0.512308	−6.4±0.2	0.39±0.07
Dis 13	1	U. Ca.	72.0[c]	N	5.9	219	2.68	2.18	7.3	1.4	0.512363±10	0.1160	0.512308	−6.4±0.2	0.30±0.08
S15/02	7	U. Ca.	72[a]	P	4.4	121	2.50	1.41	29.0	6.0	0.512390±16	0.1252	0.512333	−6.0±0.3	n.d.
S12/02	1	U. Ca.	72[a]	P	4.5	124	2.54	1.04	22.7	4.6	0.512399±10	0.1226	0.512343	−5.8±0.2	0.33±0.01
D9/98	6	U. Ca.	72[a]	P	4.2	132	2.48	1.20	36.3	7.2	0.512409±12	0.1200	0.512354	−5.5±0.2	0.27±0.07
SG/45	5	U. Ca.	72[a]	P±S	2.8	95	2.47	1.76	5.8	1.0	0.512270±12	0.1043	0.512222	−8.1±0.2	n.d.
OG-9	1	U. Ca.	72.0[c]	P	3.8	104	2.46	1.52	6.5	1.3	0.512329±18	0.1210	0.512272	−7.1±0.3	n.d.
B2/L8	1	U. Ca.	72.0[c]	P	4.1	142	2.53	1.23	39	8.3	0.512336±8	0.1287	0.512274	−7.1±0.2	n.d.
D12/01	1	U. Ca.	72.1[c]	P	5.4	113	2.40	1.92	0.068[b]	0.012[b]	0.512373±42	0.1067	0.512323	−6.2±0.8	0.45±0.02
B2/29	1	U. Ca.	72.1[c]	P	n.d.	n.d.	n.d.	n.d.	0.296[b]	0.062[b]	0.512349±13	0.1264	0.512289	−6.8±0.2	n.d.
D18/01	1	U. Ca.	72.5[c]	In	4.5	157	2.65	1.80	10.0	2.0	0.512357±1	0.1210	0.512300	−6.6±0.2	0.35±0.04
B2/L7	1	U. Ca.	72.5[c]	P	3.8	135	2.46	1.30	41.0	8.5	0.512356±10	0.1254	0.512297	−6.7±0.2	0.19±0.06
OG-11	1	U. Ca.	73[a]	P	5.6	124	2.58	1.52	6.3	1.3	0.512345±16	0.1248	0.512284	−6.9±0.3	n.d.
SG/40	5	U. Ca.	72.6[c]	P±S	3.8	153	2.56	1.27	20	4.1	0.512306±12	0.1240	0.512247	−7.6±0.2	0.25±0.07
AS-1	7	U. Ca.	73[a]	P	4.0	137	2.48	1.48	11.9	2.3	0.512384±16	0.1169	0.512328	−6.0±0.2	0.44±0.13
15/31	1	U. Ca.	73[a]	P	n.d.	n.d.	n.d.	n.d.	n.d.	n.d.	n.d.	n.d.	n.d.	n.d.	0.34±0.08
D11/01	1	U. Ca.	73[a]	S	2.2	150	2.40	1.96	5.6	1.1	0.512303±24	0.1188	0.512246	−7.6±0.4	n.d.
OG-1	1	U. Ca.	73[a]	P	5.0	150	2.62	1.11	38	8	0.512351±10	0.1273	0.512290	−6.8±0.2	n.d.
B2/L5	1	U. Ca.	73[a]	P	2.9	134	2.40	1.67	6.8	1.3	0.512368±18	0.1156	0.512312	−6.4±0.3	n.d.
B2/L4	1	U. Ca.	73.0[c]	P	3.1	131	2.32	1.40	6.7	1.4	0.512374±20	0.1264	0.512314	−6.3±0.4	n.d.
B2/L2	1	U. Ca.	73.3[c]	P	n.d.	116	2.40	1.57	8.1	1.6	0.512383±14	0.1195	0.512326	−6.1±0.3	n.d.
B2/L6	1	U. Ca.	73[a]	P	3.1	158	2.45	1.57	8.1	1.6	0.512363±10	0.1195	0.512306	−6.5±0.2	n.d.

(continued on next page)

Appendix A (*continued*)

Sample no.	Or.	Str.	*T* (Ma)	CFA phase	CO_2 (wt.%)	Sr/P ($\times 10^{-4}$)	Ca/P	(La/Sm)$_N$	Nd ($\mu g\ g^{-1}$)	Sm ($\mu g\ g^{-1}$)	$^{143}Nd/^{144}Nd$	$^{147}Sm/^{144}Nd$	$^{143}Nd/^{144}Nd_{(T)}$	$\varepsilon Nd_{(T)}$	$\delta^{44/42}Ca$
B2/L3	1	U. Ca.	73.5[c]	P	3.1	114	2.36	1.63	5.8	1.2	0.512375±22	0.1252	0.512315	−6.3±0.4	0.29±0.02
B2/L1	1	U. Ca.	73.5[c]	P	3.2	114	2.43	1.41	9.4	1.9	0.512400±20	0.1223	0.512341	−5.8±0.4	0.28±0.01
SG/32	5	U. Ca.	74.5[c]	P±S	3.3	94	2.44	1.28	6.2	1.2	0.512349±28	0.1171	0.512292	−6.7±0.4	0.30±0.04
SG/34	5	U. Ca.	74.7[c]	P±S	3.2	91	2.49	0.97	11	2.2	0.512250±10	0.1210	0.512191	−8.7±0.2	0.35±0.03
S1/71	1	U. Ca	75[a]	P	n.d.	n.d.	n.d.	n.d.	n.d.	n.d.	n.d.	n.d.	n.d.	n.d.	0.31±0.03
D2/01	1	U. Ca.	75[a]	N	5.3	n.d.	n.d.	n.d.	0.024[b]	0.0045[b]	0.512395±10	0.1134	0.512339	−5.8±0.2	0.22±0.07
D3/01	1	U. Ca.	75[a]	S	3.8	140	2.44	3.8	0.083[b]	0.016[b]	0.512303±18	0.1166	0.512246	−7.7±0.4	0.30±0.00
SG/38	5	U. Ca.	75.0[c]	P±S	3.4	89	2.43	1.31	4.5	0.9	0.512275±12	0.1210	0.512216	−8.2±0.2	n.d.
SG/15	5	U. Ca.	75.1[c]	P±S	4.1	121	2.52	0.87	40	8	0.512182±10	0.1210	0.512123	−10.1±0.2	n.d.
SG/27	5	U. Ca.	75.3[c]	P±S	3.9	96	2.46	1.22	1.2	0.25	0.512355±22	0.1260	0.512293	−6.7±0.4	n.d.
SG/12	5	U. Ca.	76.0[c]	P±S	4.5	129	2.58	0.72	27	5.8	0.512257±12	0.1299	0.512192	−8.7±0.2	n.d.
34/01p	1	U. Ca.	78[a]	P	n.d.	n.d.	n.d.	n.d.	n.d.	n.d.	n.d.	n.d.	n.d.	n.d.	0.20±0.12
34/01s	1	U. Ca.	78[a]	S	n.d.	n.d.	n.d.	n.d.	n.d.	n.d.	n.d.	n.d.	n.d.	n.d.	0.24±0.00
D14/01	1	U. Ca.	78[a]	N	6.0	160	2.70	2.85	2.5	0.47	0.512378±16	0.1240	0.512315	−6.3±0.3	0.43±0.12
D15/01	1	U. Ca.	78[a]	S	6.2	124	2.70	2.61	2.4	0.48	0.512255±16	1210	0.512193	−8.7±0.3	0.29±0.12
D30/01	1	L. Ca.	81[a]	S	3.6	122	2.42	1.83	0.913[b]	0.177[b]	0.512360±10	0.1173	0.512298	−6.6±0.2	0.01±0.11
D6/01	1	Sa.–Ca.*	83[a]	S	3.0	n.d.	n.d.	n.d.	0.665[b]	0.125[b]	0.512349±11	0.1137	0.512287	−6.8±0.2	0.04±0.04
D27/01	1	Sa.–Ca.*	83[a]	S	5.7	135	2.47	1.32	4.486[b]	1.57[b]	0.512336±10	0.1425	0.512259	−7.4±0.2	0.12±0.06
S2/02	1	Sa.–Ca.*	83[a]	N	6.0	169	2.61	1.80	4.5	0.9	0.512354±10	0.1210	0.512288	−6.8±0.2	0.28±0.01
32/01p	1	Sa.–Ca.*	83[a]	P	n.d.	n.d.	n.d.	n.d.	5.1	1.02	0.512305±10	0.1210	0.512239	−7.8±0.2	−0.02±0.11
32/01s	1	Sa.–Ca.*	83[a]	S	n.d.	n.d.	n.d.	n.d.	5.1	1.02	0.512316±8	0.1210	0.512250	−7.6±0.2	0.13±0.03
ZS/18	1	U. Co.	86[a]	P±S	6.1	179	2.65	1.43	46	9.4	0.512347±8	0.1236	0.512277	−7.0±0.2	0.24±0.10
ZS/21	1	U. Co.	86[a]	P±S	5.4	175	2.61	1.47	73	15	0.512363±8	0.1243	0.512293	−6.7±0.3	n.d.
ZS/23	1	U. Co.	86[a]	P±S	5.2	176	2.66	1.49	73	14.8	0.512358±12	0.1226	0.512289	−6.8±0.2	n.d.
Ar-2	8	L. Co.	88[a]	P±S	n.d.	109	2.54	2.19	6.3	1.15	0.512355±10	0.1104	0.512294	−6.7±0.2	0.25±0.03
Ar-10a	8	L. Co.	88[a]	P±S	4.8	112	2.56	2.11	7.0	1.28	0.512360±10	0.1106	0.512298	−6.6±0.2	0.24±0.05
Ar-10b	8	L. Co.	88[a]	P±S	4.7	113	2.68	2.28	7.2	1.3	0.512325±10	0.1092	0.512264	−7.3±0.2	0.26±0.05
Ar-21	8	L. Co.	88[a]	P±S	4.7	120	2.68	2.11	6.1	1.11	0.512349±20	0.1101	0.512288	−6.8±0.3	0.19±0.05
Ar-20c	8	L. Co.	88[a]	P±S	4.7	113	2.68	2.28	6.4	1.17	0.512345±16	0.1106	0.512284	−6.9±0.3	0.26±0.09
S31/03	8	L. Co.	88[a]	P±S	4.7	102	2.77	2.20	2.1	0.4	0.512370±8	0.1152	0.512306	−6.5±0.3	0.32±0.03
S32/03	8	L. Co.	88[a]	P±S	2.20	125	2.65	3.91	1.7	0.3	0.512391± 8	0. 1067	n.d.	−6.0±0.2	0.30±0.04
6007	4	L. Co.	88.8[c]	P±S	2.05	172	2.65	1.60	2.8	0.5	n.d.	n.d.	n.d.	n.d.	0.27±0.09
6014	4	L. Co.	88.8[c]	P±S	5.8	187	2.79	1.50	6.3	1.2	0.512314±10	0.1152	0.512247	−7.6±0.2	0.40±0.04
S33/03	8	M. Tur.	91[a]	P±S	4.4	99	2.82	1.42	56	11	0.512411±8	0.1188	0.512341	−5.8±0.2	0.02±0.03
S34/03	8	M. Tur.	91[a]	P±S	5.6	91	2.49	0.97	117	26	0.512418±8	0.1344	0.512339	−5.8±0.2	0.01±0.04
S3/02	1	M. Tur.	91[a]	N	6.1	152	2.48	0.45	880	200	0.512411±8	0.1375	0.512329	−6.0±0.2	−0.09±0.13
D1/01	6	U. Cen.	94[a]	N	5.7	104	2.52	0.93	12.79[b]	2.75[b]	0.512413±8	0.1300	0.512333	−5.9±0.2	0.02±0.06
S4/02	9	L. Cen.	96[a]	Mm	5.7	106	2.59	1.38	13.3	2.5	0.512146±12	0.1137	0.512075	−11.0±0.2	n.d.
S5/02	9	L. Cen.	96[a]	Mm	6.0	139	2.59	0.91	56	10.8	0.512121±8	0.1167	0.512047	−11.5±0.2	n.d.
D42/01	10	L. Alb.	106[a]	N	3.0	210	2.65	0.98	470	88	0.512123±10	0.1133	0.512054	−11.4±0.2	−0.07±0.01
D7/01	1	L. Alb.	106[a]	Mm	6.1	n.d.	n.d.	n.d.	18.52[b]	3.747[b]	0.512210±12	0.1224	0.512126	−10.0±0.2	0.09±0.12
D43/01	10	L. Alb.	106[a]	N	4.2	200	2.63	1.05	390	75	0.512142±10	0.1163	0.512061	−11.2±0.2	−0.04±0.02
D49/01	10	L. Alb.	106[a]	N	3.3	214	2.59	0.95	800	142	0.512148±10	0.1074	0.512074	−11.0±0.2	−0.23±0.06
S27/03	11	L. Alb.	110[a]	N	2.0	87	2.43	1.45	25	4.3	0.512065±12	0.1040	0.511992	−12.6±0.2	−0.03±0.02
D45/01	10	U. Apt.	114[a]	N	3.4	212	2.59	n.d.	615	110	0.512160±8	0.1082	0.512084	−10.8±0.2	−0.11±0.03
S26/03	11	U. Apt.	114[a]	N	5.6	177	2.58	1.21	60	11	0.512065±8	0.1108	0.511982	−11.0±0.2	n.d.
S25/03	11	L. Bar.	125[a]	N	2.3	123	2.52	0.51	32	7.0	0.512083±10	0.1323	0.511975	−12.8±0.2	−0.26±0.05
S24/03	11	L. Haut.	130[a]	N	2.3	127	2.52	0.92	5	7.4	0.512134±14	0.1279	0.512029	−11.9±0.3	−0.19±0.05

Or. — Origin of the samples; 1 — Israel (Negev); 2 — Morocco (Ganntour); 3 — Tunisia (Gafsa); 4 — Greece (Ionian zone); 5 — Egypt (Red Sea coast); 6 — Jordan (Al Abiad, Rusaifa); 7 — Syria (Er Rakheime); 8 — Turkey (Mardin–Mazidagi); 9 — S. England (Isle of Wight, Lyme Regis); 10 — SE France (Fossé Voncontien); 11 — Helvetic Alps.

L. — Lower; M. — Middle; U. — Upper; Eo — Eocene; Ma — Maastrichtian; Ca — Campanian; Sa–Ca* — Santonian–Campanian transition; Co — Coniacian; Tu — Turonian; Ce — Cenomanian; Alb — Albian; Apt — Aptian; Bar — Barremian; Haut — Hauterivian.

N — nodular; Mm — megafossil molds; S — skeletal; P — pelletal; In — intraclastic

$_{(T)}$ Initial composition at time *T* of the sample.

[a] Estimated stratigraphic ages according to the stratigraphic position of the samples in time scales of Gradstein et al. (1995) and Berggren et al. (1995).

[b] 20% glacial acid acetic dissolution; for other samples 1/3 HNO_3 dissolution was used.

[c] Numerical Sr ages.

References

Abed, A.M., 1994. Shallow marine phosphorite–chert–palygorskite association, Upper Cretaceous, Amman Formation, Jordan. In: Lijima, A., Abed, A.M., Garrison, R.E. (Eds.), Siliceous, Phosphatic and Glauconitic Sediments of the Tertiary and Mesozoic. 29th International Geological Congress Proceedings, pp. 205–224.

Afteh, S., 1989. The phosphorite resources of Syria. In: Notholt, A.J. G., Sheldon, R.P., Davidson, D.F. (Eds.), Phosphate Deposits of the World. Cambridge University Press, Cambridge, pp. 357–362.

Allen, P., Wimbledon, W.A., 1991. Correlation of NW European Purbeck–Wealden (nonmarine Lower Cretaceous) as seen from the English type-areas. Cretaceous Research 5, 511–526.

Al-Maleh, A.K., Mouty, M., 1994. Lithostratigraphy of Senonian phosphorite deposits in the Palmyridean Region and their general sedimentological and paleogeographical framework. In: Lijima, A., Abed, A.M., Garrison, R.E. (Eds.), Siliceous, Phosphatic and Glauconitic Sediments of the Tertiary and Mesozoic. 29th International Geological Congress Proceedings, Part C, pp. 225–232.

Almogi-Labin, A., Bein, A., Sass, E., 1993. Late Cretaceous upwelling system along the southern Tethys margin (Israel): interrelationship between productivity, bottom water environments, and organic matter preservation. Paleoceanography 8, 671–690.

Amakawa, H., Nozaki, Y., Alibo, D.S., Zhang, J., Fukugawa, K., Nagai, H., 2004. Neodymium isotopic variations in Northwest Pacific waters. Geochimica et Cosmochimica Acta 68, 715–727.

Amireh, B.S., 1997. Sedimentology and palaeogeography of the regressive–transgressive Kurnub Group (Early Cretaceous), of Jordan. Sedimentary Geology 112, 69–88.

Andreu, B., 1989. Le Crétacé moyen de la transversale Agadir–Nador (Maroc): précisions stratigraphiques et sédimentologiques. Cretaceous Research 10, 49–80.

Arrigo, K.R., 2005. Marine microorganisms and global nutrient cycles. Nature 437, 349–355.

Arthur, M.A., Jenkyns, H.C., 1981. Phosphorites and paleoceanography. Oceanologica Acta 4, 83–96.

Arthur, M.A., Scholle, P.A., Hasson, P., 1979. Stable isotopes of oxygen and carbon in carbonates from Sites 398 and 116 of the Deep Sea Drilling Project. In: Sibuet, J.-C., et al. (Ed.), Initial Reports of the Deep Sea Drilling Project, vol. 47. U.S. Government Printing Office, Washington, D.C., pp. 477–491. Part 2.

Ayyad, S.N., Abed, M.M., Abu Zied, R.H., 1996. Biostratigraphy and correlation of Cretaceous rocks in Gebel Arif El–Naga, northeastern Sinai, Egypt, based on planktonic foraminifera. Cretaceous Research 17, 263–291.

Barber, R.T., Smith, R.L., 1981. Coastal upwelling ecosystems. In: Longhurst, A.R. (Ed.), Analysis of Marine Ecosystems. Academic Press, New York, N.Y., pp. 31–68.

Barrera, E., Savin, S.M., 1999. Evolution of Late Campanian–Maastrichtian marine climates and oceans. In: Barrera, E., Johnson, C.C. (Eds.), Evolution of the Cretaceous Ocean–Climate System. Special Paper, vol. 332. Geological Society of America, Boulder, Colorado, pp. 245–282.

Barrera, E., Savin, S.M., Thomas, E., Jones, C.E., 1997. Evidence for thermohaline-circulation reversals controlled by sea-level change in the latest Cretaceous. Geology 25, 715–718.

Barron, E.J., 1987. Global Cretaceous paleogeography — International Geologic Correlation Program Project 191. Palaeogeography, Palaeoclimatology, Palaeoecology 59, 207–214.

Barron, E.J., Frakes, L.A., 1990. Climate model evidence for variable continental precipitation and its significance for phosphorite formation. In: Burnett, W.C., Riggs, S.R. (Eds.), Phosphate Deposits of the World. Neogene to Modern Phosphorites, vol. 3. Cambridge University Press, Cambridge, pp. 260–272.

Barron, E.J., Peterson, W.H., 1990. Mid-Cretaceous ocean circulation: results from model sensitivity studies. Paleoceanography 5, 319–337.

Barron, E.J., Harrison, C.G.A., Sloan II, J.L., Hay, W.W., 1981. Paleogeography, 180 million years ago to the present. Eclogae Geologicae Helvetiae 74, 443–470.

Barron, E.J., Hay, W.W., Thompson, S., 1989. The hydrologic cycle: a major variable during earth history. Palaeogeography, Palaeoclimatology, Palaeoecology 75, 157–174.

Baturin, G.N., 1982. Phosphorites on the Sea Floor. Origin, Composition and Distribution. Developments in Sedimentology, vol. 33. Elsevier, Amsterdam.

Baturin, G.N., Lucas, J., Prévôt-Lucas, L., 1995. Phosphorus behaviour in marine sedimentation. Continuous P-behaviour versus discontinuous phosphogenesis. Comptes Rendus de l'Académie des Sciences de Paris 321, 263–278.

Beck, R.A., Burbank, D.W., Sercombe, W.J., Riley, G.W., Barndt, J.K., Berry, J.R., Afzal, J., Khan, A.M., Jurgen, H., Metje, J., Cheema, A., Shafique, N.A., Lawrence, R.D., Khan, M.A., 1995. Stratigraphic evidence for an early collision between northwest India and Asia. Nature 373, 55–58.

Bein, A., Weiler, Y., 1976. The Cretaceous Talme Yafe Formation: a contour current shaped sedimentary prism of calcareous detritus at the continental margin of the Arabian Craton. Sedimentology 23, 511–532.

Benjamini, H., 1984. Stratigraphy of the Eocene of the Arava Valley (eastern and southern Negev, southern Israel). Israel Journal of Earth-Sciences 33, 167–177.

Bentor, Y.K., Vroman, A., 1951. The geological map of the Negev, 1:100,000. Sheet Abde (Ovda), 1st ed. Tel Aviv.

Bentor, Y.K., Vroman, A., 1954. A structural contour map of Israel (1: 250,000) with remarks on its dynamic interpretation. Bulletin of the Research Council of Israel 4, 125–135.

Berggren, W.A., Kent, D.V., Swisher, C.C., Aubry, M.-P., 1995. A revised Cenozoic geochronology and chronostratigraphy. In: Berggren, W.A., Kent, D.V., Aubry, M.-P., Hardenbol, J. (Eds.), Geochronology, Time Scales and Global Stratigraphic Correlation. SEPM Special Publication, vol. 54, pp. 129–212.

Berker, E., 1989. The Mardin–Mazidağı–Derik phosphate deposits, south-eastern Turkey. In: Notholt, A.J.G., Sheldon, R.P., Davidson, D.F. (Eds.), Phosphate Deposits of the World. Cambridge University Press, Cambridge, pp. 380–386.

Berner, E.K., Berner, R.A., 1995. Global Environment: Water, Air and Geochemical Cycles. Prentice-Hall, Upper Saddle River, NJ.

Bice, K.L., Huber, B.T., Norris, R.D., 2003. Extreme polar warmth during the Cretaceous greenhouse? The paradox of the Late Turonian $\delta^{18}O$ record at DSDP Site 511. Paleoceanography 18. doi:10.1029/2002PA000848.

Blanton, J.O., Atkinson, L.P., Pietrafesa, L.J., lee, T.N., 1981. The intrusion of Gulf Stream Water across the continental shelf due to topographically-induced upwelling. Deep-Sea Research 28A, 393–405.

Bosworth, W., Guiraud, R., Kessler II, L.G., 1999. Late Cretaceous (ca. 84 Ma) compressive deformation of the stable platform of northeast Africa (Egypt): far-field stress effects of the "Santonian event" and origin of the Syrian arc deformation belt. Geology 27, 633–636.

Boujo, A., 1976. Contribution à l'étude géologique du gisement de phosphate Crétacé–Eocène des Ganntour (Maroc occidental). Sciences Géologiques. Mémoire 43.

Brady, E.C., DeConto, R.M., Thompson, S.L., 1998. Deep water formation and poleward ocean heat transport in the warm climate extreme of the Cretaceous (80 Ma). Geophysical Research Letters 25, 4205–4208.

Bréhéret, J.-G., 1988. La francolite des concrétions phosphatées, un indicateur de diagenèse; le cas de l'Aptien–Albien du basin vocontien (SE France). Comptes Rendus de l'Académie des Sciences de Paris 306, 1017–1022.

Bréhéret, G., Delamette, M., 1989. Correlations between Mid-Cretaceous Vocontian black shales and Helvetic phosphorites in the western external Alps. In: Wiedmann, J. (Ed.), Cretaceous of the Western Tethys. Proceedings 3rd International Cretaceous Symposium, Tübingen 1987. E. Schweizerbart'sche Verlagsbuch-handlung, Stuttgart, pp. 637–655.

Broecker, W.S., Gerard, R., Ewing, M., Heezen, B.C., 1960. Natural radiocarbon in the Atlantic Ocean. Journal of Geophysical Research 65, 2903–2931.

Bush, A.B.G., 1997. Numerical simulation of the Cretaceous Tethys circumglobal current. Science 275, 807–810.

Bushinski, G.I., 1966. The origin of marine phosphorites. Lithological Mineral Resources 3, 681–699.

Butterlin, J., Vrienlick, B., Bignot, G., Clermonte, J., Colchen, M., Dercourt, J., Guiraud, R., Poisson, A., Ricou, L.-E., 1993. Lutetian (46 to 40 Ma). In: Dercourt, J., Ricou, L.E., Vrielynck, B. (Eds.), Atlas Tethys Palaeoenvironmental Maps, Explanatory Notes. Gauthier-Villars, Paris, pp. 197–209.

Camoin, G., Bellion, Y., Dercourt, J., Guiraud, R., Lucas, J., Poisson, A., Ricou, L.E., Vrielynck, B., 1993. Late Maastrichtian (69.5 to 65 Ma). In: Dercourt, J., Ricou, L.E., Vrielynck, B. (Eds.), Atlas Tethys Palaeoenvironmental Maps. BEICIP-FRANLAB, Rueil-Malmaison.

Clarke, L.J., Jenkyns, H.C., 1999. New oxygen isotope evidence for long-term Cretaceous climatic change in the Southern Hemisphere. Geology 27, 699–702.

Compton, J.S., Snyder, S.W., Hodell, D.A., 1990. Phosphogenesis and weathering of shelf sediments from the southeastern United States: implications for Miocene $\delta^{13}C$ excursions and global cooling. Geology 18, 1227–1230.

Compton, J.S., Hodell, D.A., Garrido, J.R., Mallinson, D.J., 1993. Origin and age of phosphorite from the south-central Florida Platform: relation of phosphogenesis to sea-level fluctuations and $\delta^{13}C$ excursions. Geochimica et Cosmochimica Acta 57, 131–146.

Courtney, R., White, R.S., 1986. Anomalous heat flow and geoid across the Cap Verde Rise: evidence for dynamic support from a thermal plume in the mantle. Geophysical Journal of the Royal Astronomical Society 87, 815–867.

Cook, P.J., McElhinny, M.W., 1979. A re-evaluation of the spatial and temporal distribution of sedimentary phosphate deposits in the light of plate tectonics. Economic Geology 74, 315–330.

Crowley, T.J., 1991. Past CO_2 changes and tropical sea temperatures. Paleoceanography 6, 387–394.

Delaney, L.M., Filippelli, G.M., 1994. An apparent contradiction in the role of phosphorus in Cenozoic chemical mass balances for the world ocean. Paleoceanography 9, 513–527.

De La Rocha, C.L., DePaolo, D.J., 2000. Isotopic evidence for variations in the marine calcium cycle over the Cenozoic. Science 289, 1176–1178.

Dercourt, J., Ricou, L.E., Vrielynck, B. (Eds.), 1993. Atlas Tethys Paleoenvironmental Maps. Gauthier–Villars. Paris.

Deyhle, A., MacDougall, J.D., Macisaac, C., Paytan, A., 2002. Temperature dependence of Ca isotope fractionation in marine carbonates. 12th Annual Goldschmidt Conference, Davos, Abstracts, p. A181.

D'Hondt, S., Arthur, M.A., 2002. Deep water in the Late Maastrichtian ocean. Paleoceanography 17. doi:10.1029/1999PA000486.

Dubertret, L., 1955. Carte géologique du Liban au 200,000. Beyrouth. 74 pp., 1map.

Edelman-Furstenberg, Y., 2004. Macrobenthic ecology, paleoecology and taphonomy of high-productivity systems: Upper Cretaceous Mishash Formation (Israel) and the modern Benguela system. Ph.D. Dissertation, University of Chicago, 282 pp.

Ehrenberg, S.N., Nadeau, P.H., 2002. Postdepositional, Sm/Nd fractionation in sandstones: implications for neodymium-isotope stratigraphy. Journal of Sedimentary Research 72, 304–315.

Eisenhauer, A., Gussone, N., Dietzel, M., Heuser, A., Bock, B., Böhm, F., Spero, H.J., Lea, D.W., Bijma, J., Zeebe, R., Nägler, Th.F., 2002. Kinetic effects on calcium isotope ($\delta^{44}Ca$) fractionation in calcium carbonate. 12th Annual Goldschmidt Conference, Davos, Abstracts, p. A211.

Eshet, Y., Almogi-Labin, A., 1996. Calcareous nannofossils as paleoproductivity indicators in Upper Cretaceous organic-rich sequences in Israel. Marine Micropaleontology 29, 37–61.

Falkowski, P.G., 1997. Evolution of the nitrogen cycle and its influence on the biological sequestration of CO_2 in the ocean. Science 387, 272–275.

Fanton, K.C., Holmden, C., Nowlan, G.S., Haidl, F.M., 2002. $^{143}Nd/^{144}Nd$ and Sm/Nd stratigraphy of Upper Ordovician epeiric sea carbonates. Geochimica et Cosmochimica Acta 66, 241–255.

Filippelli, G., 2001. Carbon and phosphorus cycling in anoxic sediments of the Saanich Inlet, British Columbia. Marine Geology 174, 307–321.

Filippelli, G.M., 2004. The ubiquity of phosphogenesis and the rarity of phosphorites in marine sediments. Eos AGU 85 (47), 221 (Fall Meeting Abstracts).

Filippelli, G.M., Delaney, M.L., Garrison, R.E., Omarzai, S.K., Behl, R.J., 1994. Phosphorus accumulation rates in a Miocene low oxygen basin: the Monterey Formation (Pismo Basin), California. Marine Geology 116, 419–430.

Flexer, A., Rosenfeld, A., Lipson-Benitah, S., Honigstein, A., 1986. Relative sea level changes during the Cretaceous in Israel. The American Association of Petroleum Geologists Bulletin 70, 1685–1699.

Föllmi, K.B., 1989. Evolution of the Mid-Cretaceous Triad. Lecture Notes of Earth Sciences, vol. 23. Springer-Verlag, Heidelberg.

Föllmi, K.B., 1995. 160 m.y. record of marine sedimentary phosphorus burial: coupling of climate and continental weathering under greenhouse and icehouse conditions. Geology 23, 859–862.

Föllmi, K.B., 1996. The phosphorus cycle, phosphogenesis and marine phosphate-rich deposits. Earth-Sciences Reviews 40, 55–124.

Föllmi, K.B., Delamette, M., 1991. Model simulation of Mid-Cretaceous ocean circulation: technical comments. Science 251, 94–95.

Föllmi, K.B., Garrison, R.E., Ramirez, P.C., Zambrano-Ortiz, F., Kennedy, W.J., Lehner, B.L., 1992. Cyclic phosphate-rich successions in the Upper Cretaceous of Colombia. Palaeogeography, Palaeoclimatology, Palaeoecology 93, 151–182.

Föllmi, K.B., Weissert, H., Bisping, M., Funk, H., 1994. Phosphogenesis, carbon-isotope stratigraphy, and carbonate-platform evolution along the Lower Cretaceous northern Tethyan margin. Geological Society of America Bulletin 106, 729–746.

Frank, T.D., Arthur, M.A., 1999. Tectonic forcings of Maastrichtian ocean–climate evolution. Paleoceanography 14, 103–117.

Freund, R., 1965. A model of the structural development of Israel and adjacent areas since Upper Cretaceous times. Geological Magazine 102, 337–346.

Friedrich, O., Herrle, J.O., Kößler, P., Hemleben, C., 2004. Early Maastrichtian stable isotopes: changing deep water sources in the North Atlantic? Palaeogeography, Palaeoclimatology, Palaeoecology 211, 171–184.

Froelich, P.N., Arthur, M., Burnett, W.C., Deakin, M., Hensley, V., Jahnke, R., Kaul, L., Kim, K., Roe, K., Soutar, A., Vatakanon, C., 1988. Early diagenesis of organic matter in Peru continental margin sediments: phosphorite precipitation. Marine Geology 80, 309–346.

Garrison, R.E., Kastner, M., 1990. Phosphatic sediments and rocks recovered from the Peru margin during ODP Leg 112. In: Suess, E., von Huene, R., Emeis, K. (Eds.), Proceedings of the Ocean Drilling Program. Scientific Results, vol. 112. College Station, Texas, pp. 111–134.

Garrison, R.E., Kastner, M., Reimers, C.E., 1990. Miocene phosphogenesis in California. In: Burnett, W.C., Riggs, S.R. (Eds.), Phosphate Deposits of the World. Neogene to Modern Phosphorites, vol. 3. Cambridge University Press, Cambridge, pp. 285–299.

Glenn, C.R., 1990a. Pore water, petrologic and stable carbon isotopic data bearing on the origin of Modern Peru margin phosphorites and associated authigenic phases. In: Burnett, W.C., Riggs, S.R. (Eds.), Phosphate Deposits of the World. Neogene to Modern Phosphorites, vol. 3. Cambridge University Press, Cambridge, pp. 47–61.

Glenn, C.R., 1990b. Depositional sequences of the Duwi, Sabaiya and Phosphate Formations, Egypt: phosphogenesis and glauconitization in a Late Cretaceous epeiric sea. In: Notholt, A.J.G., Jarvis, I. (Eds.), Phosphorite Research and Development. Geological Society Special Publication, vol. 52, pp. 205–222.

Glenn, C.R., Arthur, M.A., 1990. Anatomy and origin of a Cretaceous phosphorite–greensand giant, Egypt. Sedimentology 37, 123–154.

Glenn, C.R., Mansour, S.E.A., 1979. Reconstruction of the depositional and diagenetic history of phosphorites and associated rocks of the Duwi Formation (Late Cretaceous), Eastern Desert, Egypt. Annals of the Geological Survey of Egypt 9, 388–407.

Glenn, C.R., Föllmi, K.B., Riggs, S.R., Baturin, G.N., Grimm, K.A., Trappe, J., Abed, A., Galli-Olivier, C., Garrison, R., Ilyin, A.V., Jehl, C., Rohrlich, V., Sadaqah, R.M.Y., Schidlowski, M., Sheldon, R.E., Siegmund, H., 1994. Phosphorus and phosphorites: sedimentology and environments of formation. Eclogae Geologicae Helvetiae 87, 747–788.

Gordon, W.A., 1973. Marine life and ocean surface currents in the Cretaceous. Journal of Geology 81, 269–284.

Gradstein, F.M., Agterberg, F.P., Ogg, J.G., Hardenbol, J., Van Veen, P., Thierry, J., Huang, Z., 1995. A Triassic, Jurassic and Cretaceous time scale. SEPM Special Publication 54, 95–126.

Gradstein, F.M., Kaminski, M.A., Agterberg, F.P., 1999. Biostratigraphy and paleoceanography of the Cretaceous seaway between Norway and Greenland. Earth Science Reviews 46, 27–98.

Grandjean, P., Cappetta, H., Michard, A., Albarède, F., 1987. The assessment of REE patterns and $^{143}Nd/^{144}Nd$ ratios in fish remains. Earth and Planetary Science Letters 84, 181–196.

Gromet, L.P., Dymek, R.F., Haskin, L.A., Korotev, R.L., 1984. The North American shale composite: its compilation, major and trace element characteristics. Geochimica et Cosmochimica Acta 48, 2469–2482.

Guldbrandsen, R.A., 1970. Relation of carbon dioxide content of apatite of the Phosphoria Formation to regional facies. U.S. Geological Survey Professional Paper 700B, 9–13.

Gussone, N., Langer, G., Geisen, M., Eisenhauer, A., Riebesell, 2004. Ca isotope fractionation in coccolithophores. 13th Annual Goldschmidt Conference, Copenhagen, Abstracts, p. A207.

Gvirtzman, Z., 2004. Chronostratigraphic table and subsidence curves of southern Israel. Israel Journal of Earth-Sciences 53, 47–61.

Halicz, L., Galy, A., Belshaw, N.S., O'Nions, R.K., 1999. High-precision measurement of calcium isotopes in carbonates and related materials by multiple collector inductively coupled plasma mass spectrometry (MC-ICP-MS). Journal of Analytical Atomic Spectrometry 14, 1835–1838.

Hallock, P., Schlager, W., 1986. Nutrient excess and the demise of coral reefs and carbonate platforms. Palaios 1, 389–398.

Haq, B.U., 1981. Paleogene paleoceanography: Early Cenozoic oceans revisited. Oceanologica Acta. Proceedings 26th International Geological Congress, Geology of Oceans Symposium, Paris, pp. 71–82.

Haq, B.U., Hardenbol, J., Vail, P.R., 1987. Chronology of fluctuating sea levels since the Triassic. Science 235, 1156–1167.

Hay, W.W., 1995a. Cretaceous paleoceanography. Geologica Carpathica 46, 257–266.

Hay, W.W., 1995b. Paleoceanography of marine organic-carbon-rich sediments. In: Huc, A.Y., Schneidermann, N. (Eds.), Paleogeography, Paleoclimate and Source Rocks. American Association of Petroleum Geologists, Memoir, vol. 40, pp. 21–59.

Hays, J.D., Pitman III, W.C., 1973. Lithospheric plate motion, sea level changes and climatic and ecological consequences. Nature 246, 18–22.

Hein, J.R., Yeh, H.-W., Gunn, S.H., Sliter, W.V., Benninger, L.M., Wang, Ch.-H., 1993. Two major Cenozoic episodes of phosphogenesis recorded in equatorial Pacific seamount deposits. Paleoceanography 8, 293–311.

Hendriks, F., Kallenbach, H., Philobbos, E.R., 1990. Cretaceous to Early Tertiary continental and marine sedimentary environments of southeastern Egypt. Journal of African Earth Sciences 10, 229–241.

Herrle, J.O., Pross, J., Friedrich, O., Kößler, P., Hemleben, C., 2003. Forcing mechanisms for Mid-Cretaceous black shale formation: evidence from the Upper Aptian and Lower Albian of the Vocontian Basin (SE France). Palaeogeography, Palaeoclimatology, Palaeoecology 190, 399–426.

Heuser, A., Eisenhauer, A., Böhm, F., Wallmann, K., Gussone, N., Pearson, P.N., Nägler, T.F., Dullo, W.-Ch., 2005. Calcium isotope ($\delta^{44/40}Ca$) variations of Neogene planktonic foraminifera. Paleoceanography 20, PA2013. doi:10.1029/2004PA001048.

Hiatt, E.E., Budd, D.A., 2003. Extreme paleoceanographic conditions in a Paleozoic oceanic upwelling system: organic productivity and widespread phosphogenesis in the Permian Phosphoria Sea. Geological Society of America, Special Paper 370, 245–264.

Hildebrand-Mittlefehldt, N., 1985. Computerized report of all the data from the prospection drillings, 2 vols. PAMA Ltd.

Hippler, D., Gussone, N., Darling, K., Eisenhauer, A., Nagler, T.F., 2002. $\delta^{44}Ca$ in *N. pachy* (left): a new SST-proxy in polar regions. 12th Annual Goldschmidt Conference, Davos, Abstracts, p. A331.

Holmden, C., Creaser, R.A., Muehlenbachs, K., Bergstrom, S.M., Leslie, S.A., 1996. Isotopic and elemental systematics of Sr and Nd in 454 Ma biogenic apatites: implications for paleoseawater studies. Earth and Planetary Science Letters 142, 425–437.

Howarth, M.K., 1981. Palaeogeography of the Mesozoic. In: Cokes, L.R.M. (Ed.), The Evolving Earth. Cambridge University Press, Cambridge, pp. 197–220.

Huber, B.T., Hodell, D.A., Hamilton, C.P., 1995. Middle–Late Cretaceous climate of the southern high latitudes: stable isotopic evidence for minimal equator-to-pole thermal gradients. Geological Society America Bulletin 107, 1164–1191.

Ibrahim, M.I.A., 2002. Late Albian–Middle Cenomanian palynofacies and palynostratigraphy, Abu Gharadig-5 well, Western Desert, Egypt. Cretaceous Research 23, 775–788.

Ilyin, A.V., 1994. Cenomanian phosphorites in the former Soviet Union. Sedimentary Geology 94, 109–127.

Ingall, E.D., Van Cappellen, P., 1989. Relation between sedimentation rate and burial of organic phosphorus and organic carbon in marine sediments. Geochimica et Cosmochimica Acta 54, 373–386.

Isaacs, C.M., Pisciotto, K.A., Garrison, R.E., 1983. Siliceous deposits in the Pacific region. In: Iijima, A., Hein, J.R., Siever, R. (Eds.), Developments in Sedimentology, vol. 36. Elsevier, Amsterdam, pp. 247–282.

Issawi, B., 1973. Nubia sandstone: type section. The American Association of Petroleum Geologists Bulletin 57, 741–745.

Issawi, B., 1989. A review of Egyptian Late Cretaceous phosphate deposits. In: Notholt, A.J.G., Sheldon, R.P., Davidson, D.F. (Eds.), Phosphate Deposits of the World. Cambridge University Press, Cambridge, pp. 187–193.

Jacobsen, S.B., Wasserburg, G.J., 1980. Sm–Nd isotopic evolution of chondrites. Earth and Planetary Science Letters 50, 139–155.

Jahnke, R.A., Emerson, S.R., Roe, K.K., Burnett, W.C., 1983. The present day formation of apatite in Mexican continental margins sediments. Geochimica et Cosmochimica Acta 47, 259–266.

Jallad, I.S., Abu Murrey, O.S., Sadaqah, R.M., 1989. Upper Cretaceous phosphorites of Jordan. In: Notholt, A.J.G., Sheldon, R.P., Davidson, D.F. (Eds.), Phosphate Deposits of the World. Cambridge University Press, Cambridge, pp. 344–351.

Jarvis, I., 1992. Sedimentology, geochemistry and origin of phosphate chalks: the Upper Cretaceous deposits of NW Europe. Sedimentology 39, 55–97.

Jarvis, I., Burnett, W.C., Nathan, Y., Almbaydin, F.S.M., Attia, A.K. M., Castro, L.N., Flicoteaux, R., Hilmy, M.E., Husain, V., Qutawnah, A.A., Serjani, A., Zanin, Y.N., 1994. Phosphorite geochemistry: state-of-the-art and environmental concerns. Eclogae Geologicae Helvetiae 87, 643–700.

Jasinski, S.M., 2003. Phosphate rock. U.S. Geological Survey Minerals Yearbook, pp. 56.1–56.5.

Jeandel, C., 1993. Concentration and isotopic composition of Nd in the South Atlantic waters. Earth and Planetary Science Letters 117, 581–591.

Jewell, P.W., 1995. Geological consequences of global encircling equatorial currents. Geology 23, 117–120.

Kaiho, K., Saito, S., 1994. Oceanic crust production and climate during the last 100 Myr. Terra Nova 6, 376–384.

Kennedy, W.J., Garrison, R.E., 1975. Morphology and genesis of nodular phosphates in the Cenomanian glauconite marl of south east England. Lethaia 8, 339–360.

Kerr, A.C., 1998. Oceanic plateau formation: a cause of mass extinction and black shale deposition around the Cenomanian–Turonian boundary? Journal of the Geological Society, London 155, 619–626.

Kerr, A.R., 2002. Inconstant ancient seas and life's path. Science 298, 1165–1166.

Keto, L.S., Jacobsen, S.B., 1988. Nd isotopic variations of Phanerozoic paleoceans. Earth and Planetary Science Letters 90, 395–410.

Kinsey, D.W., Davies, P.J., 1979. Effects of elevated nitrogen and phosphorus on coral reef growth. Limnology and Oceanography 24, 935–940.

Klitzsch, E.H., Squyres, C.H., 1990. Paleozoic and Mesozoic geological history of northeastern Africa based upon new interpretation of Nubian strata. The American Association of Petroleum Geologists Bulletin 74, 1203–1211.

Knight, R.I., 1999. Phosphates and phosphogenesis in the Gault Clay (Albian) of the Anglo-Paris Basin. Cretaceous Research 20, 507–521.

Kolodny, Y., 1980. Carbon isotopes and depositional environment of a high productivity sedimentary sequence — the case of the Mishash–Ghareb formations, Israel. Israel Journal of Earth-Sciences 29, 147–156.

Kolodny, Y., Garrison, R.E., 1994. Sedimentation and diagenesis in paleo-upwelling zones of epeiric sea and basinal settings: a comparison of the Cretaceous Mishash Formation of Israel and the Miocene Monterey Formation of California. In: Lijima, A., Abed, A.M., Garrison, R.E. (Eds.), Siliceous, Phosphatic and Glauconitic Sediments of the Tertiary and Mesozoic. 29th International Geological Congress Proceedings, pp. 133–158.

Kolodny, Y., Raab, M., 1988. Oxygen isotopes in phosphatic fish remains from Israel: paleothermometry of tropical Cretaceous and Tertiary shelf waters. Palaeogeography, Palaeoclimatology, Palaeoecology 64, 59–67.

Krajewski, K.P., Van Cappellen, P., Trichet, J., Kuhn, O., Lucas, J., Martin-Algarra, A., Prévôt, L., Tewari, V.C., Gaspar, L., Knight, R. I., Lamboy, M., 1994. Biological processes and apatite formation in sedimentary environments. Eclogae Geologicae Helvetiae 87, 701–745.

Kump, L.P., 1990. Neogene geochemical cycles: implications concerning phosphogenesis. In: Burnett, W.C., Riggs, S.R. (Eds.), Phosphate Deposits of the World. Neogene to Modern Phosphorites, vol. 3. Cambridge University Press, Cambridge, pp. 273–282.

Larson, R.L., 1991. Latest pulse of Earth: evidence for a Mid-Cretaceous superplume. Geology 19, 547–550.

Larson, R.L., Erba, E., 1999. Onset of the Mid-Cretaceous greenhouse in the Barremian–Aptian: igneous events and the biological, sedimentary, and geochemical responses. Paleoceanography 14, 663–678.

Lécuyer, C., Reynard, B., Grandjean, P., 2004. Rare earth element evolution of Phanerozoic seawater recorded in biogenic apatites. Chemical Geology 204, 63–102.

Lewy, Z., 1990. Transgressions, regressions and relative sea level changes on the Cretaceous shelf of Israel and adjacent countries. A critical evaluation of Cretaceous global sea level correlations. Paleoceanography 5, 619–637.

Lewy, Z., 2001. Campanian Ammonites from the Mishash Formation (southern Israel) and their implication on Ammonoid mode of life and functional morphology Geological Survey of Israel, Report GSI/38/01.

Li, L., Keller, G., 1999. Variability in Late Cretaceous climate and deep waters: evidence from stable isotopes. Marine Geology 161, 171–190.

Lloyd, C.R., 1982. The Mid-Cretaceous earth: palaeogeography, ocean circulation and temperature, atmospheric circulation. Journal of Geology 90, 393–413.

Lucas, J., Prévôt-Lucas, L., 1995. Tethyan phosphates and bioproductites. In: Naim, et al. (Ed.), The Oceans Basins and Margins. The Tethys Ocean, vol. 8. Plenum Press, New York, pp. 367–391.

Luyendyk, B., Forsyth, D., Phillips, J.D., 1972. Experimental approach to the paleocirculation of the oceanic surface waters. Geological Society of America Bulletin 83, 2649–2664.

Mackenzie, F.T., Ver, L.M., Sabine, C., Lane, M., Lerman, A., 1993. C, N, P, S global biogeochemical cycles and modeling of global change. In: Wollast, R., Mackenzie, F.T., Chou, L. (Eds.), Interactions of C, N, P and S Biogeochemical Cycles and Global Change. Springer-Verlag, Berlin, pp. 1–61.

Mahoney, J., Nicollett, C., Dupuy, C., 1991. Madagascar basalts: tracking oceanic and continental sources. Earth and Planetary Science Letters 104, 350–363.

Mallinson, D.J., Compton, J.S., 1997. Linking phosphogenic episodes on the southeast U.S. margin to marine $\delta^{13}C$ and $\delta^{18}O$ records. Geology 25, 103–106.

Martin, E.E., Scher, H.D., 2004. Preservation of seawater Sr and Nd isotopes in fossil fish teeth: bad news and good news. Earth and Planetary Science Letters 220, 25–39.

Massaad, M., 1976. Origin and environment of deposition of Lebanon basal sandstones. Eclogae Geologicae Helvetiae 69, 85–91.

Masse, J.P., Bellion, Y., Benkhelil, J., Ricou, L.-E., Dercourt, J., Guiraud, R., 1993. Early Aptian (114 to 111 Ma). In: Dercourt, J., Ricou, L.E., and Vrielynck, B. (Eds.), Atlas Tethys Palaeoenvironmental Maps, Explanatory Notes. Gauthier-Villars, Paris, pp. 135–152.

Mateer, N.J., Wycisk, P., Jacobs, L.L., Brunet, M., Luger, P., Arush, M.A., Hendricks, F., Weissbrod, T., Gvirtzman, G., Mbede, E., Dina, A., Moody, R.T.J., Weigelt, G., El-Nakhal, H.A., Hell, J., Stets, J., 1992. Correlation of nonmarine Cretaceous strata of Africa and the Middle East. Cretaceous Research 13, 273–318.

Matsumoto, T., 1980. Inter-regional correlation of transgressions and regressions in the Cretaceous period. Cretaceous Research 1, 359–373.

McArthur, J.M., Howarth, R.J., Bailey, T.R., 2001. Strontium isotope stratigraphy: LOWESS Version 3. Best-fit line to the marine Sr-isotope curve for 0 to 509 Ma and accompanying look-up table for deriving numerical age. Journal of Geology 109, 155–169.

McKelvey, V.E., Williams, J.S., Sheldon, R.P., Cressman, E.R., Cheney, T.M., Swanson, R.W., 1959. The Phosphoria, Park City and Shedhorn Formations in the Western Phosphate Field. US Geological Survey Professional Paper 313-A.

Miller, K.G., Kominz, M.A., Browning, J.V., Wright, J.D., Mountain, G.S., Katz, M.E., Sugarman, P.J., Cramer, B.S., Christie-Blick, N., Pekar, S.F., 2005. The Phanerozoic Record of Global Sea-Level Change. Science 310, 1293–1298.

Molina-Cruz, A., 1977. The relation of the southern trade winds to upwelling processes during the last 75,000 years. Quaternary Research 8, 324–338.

Moshkovitz, S., Ehrlich, A., Soudry, D., 1983. Siliceous microfossils of the Upper Cretaceous Mishash Formation, central Negev, Israel. Cretaceous Research 4, 173–194.

Moshrif, M.A., 1980. Recognition of fluvial environments in the Biyadth–Wasia sandstones (Lower–Middle Cretaceous) as revealed by textural analysis. Journal of Sedimentary Petrology 50, 603–612.

Nägler, Th.F., Eisenhauer, A., Müller, A., Hemleben, C., Kramers, J., 2000. The $\delta^{44}Ca$-temperature calibration on fossil and cultured *Globigerinoides sacculifer*: new tool for reconstruction of past sea surface temperatures. Geochemistry, Geophysics, Geosystems 1, 1–9.

Nathan, Y., Shiloni, Y., Roded, R., Gal, I., Deutsch, Y., 1979. The geochemistry of the northern and central Negev phosphorites. Geological Survey of Israel, Bulletin 73.

Nathan, Y., Soudry, D., Levy, Y., Shitrit, D., Dorfman, E., 1997. Geochemistry of cadmium in the Negev phosphorites. Chemical Geology 142, 87–107.

Nathan, Y., Soudry, D., Glenn, C., Shenker, M., Huang, X.L., Schilman, B., 2006. C/P organic ratios in phosphorites and related facies. European Geosciences Union General Assembly, Vienna, Abstracts.

Norris, R.D., Bice, K.L., Magno, E.A., Wilson, P.A., 2002. Jiggling the tropical thermostat during the Cretaceous hot house. Geology 30, 299–302.

Notholt, A.J.G., Sheldon, R.P., Davidson, D.F., 1989. Phosphate Deposits of the World. Phosphate Rock Resources, vol. 2. Cambridge University Press, Cambridge.

Parrish, J.T., Curtis, R.L., 1982. Atmospheric circulation, upwelling, and organic-rich rocks in the Mesozoic and Cenozoic eras. Palaeogeography, Palaeoclimatology, Palaeoecology 40, 31–66.

Philip, J., Babinot, J.-F., Tronchetti, G., Fourcade, E., Ricou, L.-E., Guiraud, R., Bellion, Y., Herbin, J.-P., Combes, P.-J., Cornee, J.-J., Dercourt, J., 1993. Late Cenomanian (94–92 Ma). In: Dercourt, J., Ricou, L.E., Vrielynck, B. (Eds.), Atlas Tethys palaeoenvironmental maps, explanatory notes. Gauthier-Villars, Paris, pp. 153–178.

Piepgras, D.J., Wasserburg, G.J., 1982. Isotopic composition of neodymium in waters from the Drake passage. Science 217, 207–217.

Pisciotto, K.A., Garrison, R.E., 1981. Lithofacies and depositional environments of the Monterey Formation, California. In: Garrison, R.E., Douglas, R.G. (Eds.), The Monterey Formation and Related Siliceous Rocks of California. Society of Economic Paleontologists and Mineralogists Publication, Pacific Section, pp. 97–122.

Pomini-Papaioannou, F., 2001. Lithostratigraphy–Sedimentology of the Upper Cretaceous Phosphatic Formations of the Ionian Zone: Mechanism of Phosphatization — Paleotectonic frame. Department of Geology, University of Athens, Gaia, vol. 9.

Poulsen, C.J., Seidov, D., Barron, E.J., Peterson, W.H., 1998. The impact of paleogeographic evolution on the surface oceanic circulation and the marine environment within the Mid-Cretaceous Tethys. Paleoceanography 13, 546–559.

Poulsen, C.J., Barron, E.J., Arthur, M.A., Peterson, W.H., 2001. Response of the Mid-Cretaceous global oceanic circulation to tectonic CO_2 forcings. Paleoceanography 16, 576–592.

Poulsen, C.J., Gendaszek, A.S., Jacob, R.L., 2003. Did the rifting of the Atlantic Ocean cause the Cretaceous thermal maximum? Geology 31, 115–118.

Prévôt, L., 1988. Geochemistry, petrography, genesis of Cretaceous–Eocene phosphorites. The Ganntour deposit (Morocco): a type example. Mémoires de la Société Géologique de France 158.

Price, G.D., Sellwood, B.W., Corfield, R.M., Clarke, L., Cartlidge, J., 1998. Isotopic evidence for palaeotemperatures and depth stratification of Middle Cretaceous planktonic foraminifera from the Pacific Ocean. Geological Magazine 135, 183–191.

Pucéat, E., Lécuyer, C., Reisberg, L., 2005. Neodymium isotope evolution of NW Tethyan upper ocean waters throughout the Cretaceous. Earth and Planetary Science Letters 236, 705–720.

Reiss, Z., 1988. Assemblages from a Senonian high-productivity sea. Revue de Paléobiologie 2, 323–332.

Reynard, B., Lécuyer, C., Grandjean, P., 1999. Crystal–chemical controls on rare-earth element concentrations in fossil biogenic

apatites and implications for paleoenvironmental reconstructions. Chemical Geology 155, 231–241.

Riddler, G.P., Van Eck, M., Farasani, A.M., 1989. The phosphorite deposits of the Sirhan–Turayf region, northern Saudi Arabia. In: Notholt, A.J.G., Sheldon, R.P., Davidson, D.F. (Eds.), Phosphate Deposits of the World. Cambridge University Press, Cambridge, pp. 332–337.

Riggs, S., 1984. Paleoceanographic model of Neogene phosphorite deposition, U.S. Atlantic continental margin. Science 223, 123–131.

Riggs, S.R., Snyder, St.W., Snyder, S.W., Hine, A.C., 1990. Stratigraphic framework for cyclical deposition of Miocene sediments in the Carolina phosphogenic province. In: Burnett, W.C., Riggs, S.R. (Eds.), Phosphate Deposits of the World. Neogene to Modern Phosphorites, vol. 3. Cambridge University Press, Cambridge, pp. 381–395.

Robaszynski, F., Poels, J.P., Martin, M., 1988. Le gisement de craie phosphatée de Ciply: données nouvelles. Bulletin de la Société Belge de Géologie 97, 9–24.

Ronov, A.B., 1994. Phanerozoic transgressions and regressions on the continents: a quantitative approach based on areas flooded by the sea and areas of marine and continental deposition. American Journal of Sciences 294, 777–801.

Ruffell, A.H., 1995. Seismic stratigraphic analysis of non-marine Lower Cretaceous strata in the Wessex and North Celtic Sea Basins. Cretaceous Research 16, 603–637.

Ruttenberg, K.C., Berner, R.A., 1993. Authigenic apatite formation and burial in sediments from non-upwelling, continental margin environments. Geochimica et Cosmochimica Acta 57, 991–1007.

Salvan, H.M., 1985. Particularités de répartition stratigraphique des dépôts phosphatés de la Mésogée et de la bordure atlantique du continent africain. Nouvelles possibilités d'interprétation. Sciences Géologiques, Mémoire 77, 93–98.

Sarnthein, M., Tetzlaff, G., Koopmann, B., Wolter, K., Pflaumann, U., 1981. Glacial and interglacial wind regimes over the eastern subtropical Atlantic and North-West Africa. Nature 293, 193–196.

Sass, E., Bein, A., 1982. The Cretaceous carbonate platform in Israel. Cretaceous Research 3, 135–144.

Schlanger, S.O., Jenkyns, H.C., Premoli-Silva, I., 1981. Volcanism and vertical tectonics in the Pacific basin and related to global Cretaceous transgressions. Earth and Planetary Science Letters 52, 435–449.

Schlesinger, W.H., 1997. Biogeochemistry, an Analysis of Global Change. Academic Press, San Diego.

Schmitt, A.-D., Chabaux, F., Stille, P., 2003a. The calcium riverine and hydrothermal isotopic fluxes and the oceanic calcium mass balance. Earth and Planetary Science Letters 213, 503–518.

Schmitt, A.-D., Stille, P., Venneman, T., 2003b. Variations of the $^{44}Ca/^{40}Ca$ ratio in seawater during the past 24 million years: evidence from $\delta^{44}Ca$ and $\delta^{18}O$ values of Miocene phosphates. Geochimica et Cosmochimica Acta 67, 2607–2614.

Schulze, F., Marzouk, A.M., Bassiouni, M.A.A., Kuss, J., 2004. The Late Albian–Turonian carbonate platform succession of west-central Jordan: stratigraphy and crises. Cretaceous Research 25, 709–737.

Schouten, S., Hopmans, E.C., Forster, A., van Breugel, Y., Kuypers, M.M., Sinninghe, D., 2003. Extremely high sea-surface temperatures at low latitudes during the Middle Cretaceous as revealed by archeal membrane lipids. Geology 31, 1069–1072.

Scotese, C.R., Gahagan, L.M., Larson, R.L., 1988. Plate tectonic reconstructions of the Cretaceous and Cenozoic ocean basins. Tectonophysics 155, 27–48.

Shaw, H.F., Wasserburg, G.J., 1985. Sm–Nd in marine carbonates and phosphates: implications for Nd isotopes in seawater and crustal age. Geochimica et Cosmochimica Acta 49, 503–518.

Sheldon, R.P., 1964. Paleolatitudinal and paleogeographic distribution of phosphorite. US Geological Survey Professional Paper 501C, 106–113.

Sheldon, R.P., 1980. Episodicity of phosphate deposition and deep-ocean circulation. An hypothesis. In: Bentor, Y.K. (Ed.), Marine Phosphorites, Geochemistry, Occurrence, Genesis. SEPM, Special Publication, vol. 29, pp. 239–247.

Shemesh, A., 1986. Stable isotopes and rare earth elements in phosphatic rocks. Unpublished PhD thesis, Hebrew University, Jerusalem.

Shemesh, A., Kolodny, Y., 1988. Oxygen isotope variations in phosphorites from the southeastern Tethys. Israel Journal of Earth-Sciences 37, 1–15.

Shields, G., Stille, P., Brasier, M.D., 2000. Isotopic records across two phosphorite giant episodes compared: the Precambrian–Cambrian and the Late Cretaceous–Recent. In: Glenn, C.R., Prévôt-Lucas, L., Lucas, J. (Eds.), Marine Authigenesis: from Global to Microbial. SEPM Special Publication, vol. 66, pp. 103–115.

Simkiss, K., 1964. Phosphates as crystal poisons of calcification. Biological Review 39, 487–505.

Skulan, J., DePaolo, D.J., Owens, T.L., 1997. Biological control of calcium isotopic abundances in the global calcium cycle. Geochimica et Cosmochimica Acta 61, 2505–2510.

Slansky, M., 1980. Géologie des phosphates sédimentaires. Bureau de Recherches Géologiques et Minières 114.

Smith, A.G., Hurley, A.M., Briden, J.C., 1981. Phanerozoic Paleocontinental World Maps. Cambridge University Press, Cambridge.

Snyder, S.W., Hine, A.C., Riggs, S.R., 1990. The seismic stratigraphic record of shifting Gulf Stream flow paths in response to Miocene glacio-eustacy: implications for phosphogenesis along the North Carolina continental margins. Phosphate Deposits of the World. Neogene to Modern Phosphorites, vol. 3. Cambridge University Press, Cambridge, pp. 396–423.

Soudry, D., 1987. Ultra-fine structures and genesis of the Campanian Negev high-grade phosphorites (southern Israel). Sedimentology 34, 641–660.

Soudry, D., Eyal, A., 1994. Har Nishpe phosphate deposit. Summary of geological survey 1993. Geological Survey of Israel Report GSI/16/94, and Rotem Deshanim, Report G/05/07/94.

Soudry, D., Moshkovitz, S., Ehrlich, A., 1981. Occurrence of siliceous microfossils (diatoms, silicoflagellates and sponge spicules) in the Campanian Mishash Formation, southern Israel. Eclogae Geologicae Helvetiae 74, 97–107.

Soudry, D., Nathan, Y., Roded, R., 1985. The Ashosh–Haroz facies and their significance for the Mishash palaeogeography and phosphorite accumulation in the northern and central Negev. Israel Journal of Earth-Sciences 34, 211–220.

Soudry, D., Ehrlich, S., Yoffe, O., Nathan, Y., 2002. Uranium oxidation state and related variations in geochemistry of phosphorites from the Negev (southern Israel). Chemical Geology 189, 213–230.

Soudry, D., Segal, I., Nathan, Y., Glenn, C.R., Halicz, L., Lewy, Z., VonderHaar, D.L., 2004. $^{44}Ca/^{42}Ca$ and $^{143}Nd/^{144}Nd$ isotope variations in Cretaceous–Eocene Tethyan francolites and their bearing on phosphogenesis in the southern Tethys. Geology 32, 389–392.

Soudry, D., Nathan, Y., Glenn, CR., 2005. Phosphorus accumulation rates in the Upper Cretaceous–Eocene of the southern Tethys

margin — a case study of temporal fluctuations in phosphogenesis and rates of phosphate fluxes. Final scientific report. Submitted to the US–Israel Binational Science Foundation. Geological Survey Israel, Report GSI/01/2005.

Stille, P., 1992. Nd–Sr isotope evidence for dramatic changes of paleocurrents in the Atlantic Ocean during the past 80 m.y. Geology 20, 387–390.

Stille, P., Steinmann, M., Riggs, S.R., 1996. Nd isotope evidence for the evolution of the paleocurrents in the Atlantic and Tethys Oceans during the past 180 Ma. Earth and Planetary Science Letters 144, 9–19.

Tachikawa, K., Jeandel, C., Roy-Barman, 1999. A new approach to the Nd residence time in the ocean: the role of atmospheric inputs. Earth and Planetary Science Letters 170, 433–446.

Thiede, J., Suess, E., 1983. Sedimentary record and ancient coastal upwelling. Episodes 2, 15–18.

Thierstein, H.R., 1979. Paleoceanographic implications of organic carbon and carbonate distribution in Mesozoic deep sea sediments. In: Talwani, M., Hay, W., Ryan, W.B.F. (Eds.), Deep Drilling Results in the Atlantic Ocean. American Geophysical Union, Maurice Ewing Series, vol. 3, pp. 249–274.

Thomas, D.J., Bralower, T.J., Jones, C.E., 2003. Neodymium isotopic reconstruction of Late Paleocene–Early Eocene thermohaline circulation. Earth and Planetary Science Letters 209, 309–322.

Trappe, J., 1991. Stratigraphy, facies distribution and paleogeography of the marine Paleogene from the Western High Atlas, Morocco. Neus Jahrbuch für Geologie und Palaontologie 180, 279–321.

Tyson, R.V., Funnell, B.M., 1987. European Cretaceous shorelines, stage by stage. Palaeogeography, Palaeoclimatology, Palaeoecology 59, 69–91.

Van Cappellen, P., Ingall, D., 1996. Redox stabilization of the atmosphere and oceans by phosphorus-limited marine productivity. Science 271, 493–496.

Watts, A.B., Bodine, J.H., Ribe, N.M., 1980. Observations of flexure and the geological evolution of the Pacific Ocean Basin. Nature 283, 532–537.

Weaver, C., Pollard, L.D., 1973. The Chemistry of Clay Minerals. Developments in Sedimentology, vol. 15. Elsevier Scientific Publishing Co., Amsterdam, New York.

Weissbrod, T., Perath, I., 1990. Criteria for the recognition and correlation of sandstone units in the Precambrian and Paleozoic–Mesozoic clastic sequence in the Near East. Journal of African Earth Sciences 10, 253–270.

Wiedmann, V.J., Butt, A., Einsele, G., 1978. Vergleich von marokkanischen Kreide-Küstenaufschlussen und Tiefseebohrungen (DSDP): Stratigraphie, Paläoenvironment and Subsidenz an einem passiven Kontinentalrand. Geologische Rundschau 67, 454–508.

Wilkinson, B.H., Algeo, T.J., 1989. Sedimentary carbonate record of calcium–magnesium cycling. American Journal of Sciences 289, 1158–1194.

Wilson, P.A., Norris, R.D., 2001. Warm tropical ocean surface and global anoxia during the Mid-Cretaceous period. Nature 412, 425–429.

Winterer, E.L., 1991. The Tethyan Pacific during Late Jurassic and Cretaceous times. Palaeogeography, Palaeoclimatology, Palaeoecology 87, 253–265.

Yarkoni, M., 1985. Hydroelectric Plant Mediterranean–Dead Sea (The Main Tunnel), Drillcore M-13. Tahal Engineering and Consulting Ltd., Report 04/85/4.

Zhu, P., Macdougall, J.D., 1998. Calcium isotopes in the marine environment and the oceanic calcium cycle. Geochimica et Cosmochimica Acta 62, 1691–1698.